Active Human Body Models for Capturing Variability in Occupant Bracing in Pre-Crash Braking and Low-Speed Impact Events

Karan S. Devane, Hana Chan, Devon L. Albert, Andrew R. Kemper, F. Scott Gayzik

Abstract The objective of this study was to assess an active finite element human body model's capability of capturing variability in occupant bracing. This study used the Global Human Body Models Consortium midsize-male simplified occupant model with active musculature. This model uses a PID-controlled muscle activation strategy with joint angles as control variables. The physiological cross-sectional area (PCSA), reaction delay, and PID-controller reference joint angles were varied to assess their effect on model response. A total of 56 simulations were carried out. Data from five 50th-percentile male volunteers in braced muscle states were used to compare the model performance. Peak forward excursions for various body markers, reaction forces, and average CORA scores were extracted from each simulation and were compared against experimental data. The model was able to capture the variation in occupant bracing by varying PCSA and reference joint angles in the model. The effect of reference joint angle on reaction forces, peak forward excursions, and CORA score was larger than that of PCSA and reaction delay and was statistically significant, making it a better choice. This study provides novel methods and models to capture variation in occupant bracing, which will be useful for studying its effect on injury risk in vehicle crashes.

Keywords Computational model, active muscle, occupant bracing, pre-crash braking, low-speed impact.

I. INTRODUCTION

Active Finite Element Human Body Models (AHBMs) have gained popularity over the last few years due to their ability to better predict occupant kinematics in low-speed impacts and pre-crash scenarios compared to their passive counterparts [1-5]. These models are one of the tools that are helping to design new restraint systems and that consider the change in posture due to pre-crash countermeasures or occupant pre-crash bracing [5,6]. Previous literature has shown how changes in posture and muscle bracing affect the efficacy of safety systems [4,7-9]. Some studies have also reported increased risk to the occupants and pedestrians due to muscle bracing in motor vehicle crashes [10,11].

Numerous experimental studies have evaluated volunteer responses in varying levels of muscle activity or state [9,12-17]. In the study by Osth et al. [9], the authors reported a decrease in head CG forward excursion due to increased muscle activity in the cervical and lumbar muscles during driver-initiated braking compared to autonomous braking. Beeman et al. [12] and Chan et al. [13,14] observed similar behaviour in volunteers during laboratory sled tests where the volunteers were asked to brace themselves before being exposed to a braking or low-speed impact acceleration pulse. Albert et al. [18] reported that the magnitude of the bracing variability observed between 20 male and female subjects was correlated to the differences in the occupant kinematics. The study also observed different bracing strategies before the sled pulse and suggested the need for future studies to assess the effect of different bracing strategies and magnitudes on occupant response.

When it comes to assessing the effect of numerous variables on occupant response, parametric computational studies provide cost- and time-effective approaches that have been utilized by previous researchers [5,6,19,20]. To use any HBM or AHBM in the design of experimental (DOE) studies, it is necessary to validate and verify their response using experimental data. These models should be robust and accurate enough to handle all the various scenarios to be simulated in the DOE. To the author's knowledge, there are no other studies that have assessed the ability of AHBMs to capture variability in occupant bracing or used them to study the effects of bracing

K. S. Devane is a Research Assistant Professor (phone: +1 336 716 3260, email: kdevane@wakehealth.edu) and F. S. Gayzik is a Professor of Biomedical Engineering in the Center for Injury Biomechanics at the Wake Forest University School of Medicine in Winston-Salem, NC, USA. A. R. Kemper is an Associate Professor, H. Chan is a PhD student, and D. L. Albert is a Research Assistant Professor of Biomedical Engineering in the Center for Injury Biomechanics at Virginia Tech in Blacksburg, VA, USA.

variability on occupant response. Therefore, the objective of this study was to assess the Global Human Body Models Consortium (GHBMC) mid-size male model's capability to capture the variation in occupant bracing using three different strategies that capture variability in bracing.

II. METHODS

Experimental Testing

To compare the model response and verify the suitability of the AHBM to simulate pre-crash braking and low-speed impact events, experimental data from five mid-size male volunteers (age: 23.4±2.3 years, height: 174.5±3.5 cm, weight: 77.1±3.2 kg) were used in this study [13,14,21]. Each volunteer was subjected to two pulse severities (1.0g and 2.5g) and two muscle states (relaxed and braced) in the frontal direction. For the comparison purpose of this study, only the braced muscle state experimental data were used. In addition, only the data from the volunteers who were subjected to braced muscle state experimental conditions for both pulse severities on the first day were considered for this study to avoid the effects of acclimation [6,13]. Each volunteer was instrumented to measure bilateral occupant kinematics and muscle activation using a VICON motion capture and surface electromyography (EMG), respectively. Reaction forces at the contacting surfaces were measured using multi-axis load cells. Additional details regarding the experimental procedures are reported in the previous studies [13,14,21]. All test procedures were reviewed and approved by the Virginia Tech institutional review board (IRB #17-1008).

Computational Modeling

The GHBMC simplified occupant mid-size male model (M50-OS+Active v2.3) with active musculature was used in this study [1,2]. This active model uses a joint-angle-based PID-controlled strategy to calculate muscle activation for posture maintenance. Only the neck muscles use both muscle length and joint angle for the PID controllers. The model was gravity-settled and belted in a rigid buck to simulate pre-crash braking and low-speed impact events in a braced muscle state. The procedure used to simulate the braced muscle condition using higher target joint angles than initial posture target angles is explained in previous studies [2,22,23]. The acceleration pulses used for simulating pre-crash braking and low-speed impact were taken from Chan et al. [13]. The simulation setup is shown in Fig. 1.

Fig. 1. Simulation setup for simulating pre-crash braking and low-speed impact events using M50-OS+Active.

To assess the active model's ability to capture the variability in occupant bracing a design of experiments (DOE) was performed by varying physiological cross-sectional area (PCSA), reaction delay [1,24], and target joint angles. The forces generated by muscles are directly proportional to the PCSA. For joint angles, the muscle forces will increase as the error between the target joint angle and the measured joint angle increases. For reaction delay, a longer reaction delay increases the muscle activation onset time, which delays the occupant's reaction to a perturbation. The PCSA was included in the study because individuals with similar height and mass can have different muscle masses, which can affect the muscle forces generated by each subject. Similarly, it has been reported by many studies that the reaction times of subjects vary based on the muscle activation onset times [9,13,25]. Therefore, reaction delay was included as one of the variables to study. Setting target joint angles higher than the initial posture angles to brace the model against contact surfaces is a computational trick that has been proven effective in modeling braced occupants [2,23]. This method helps AHBMs that use a PID-

controlled closed-loop muscle activation system to model reflexive feedback control to intentionally brace against contact surfaces. When volunteers are asked to brace themselves against the sled buck, they push against all the contacting surfaces by extending their arms, legs, and torso, effectively increasing their joint angles beyond their current positions. Kato et al. [3] have used reaction forces at the contact surfaces as a control variable for the PID controllers to model bracing which adds another layer of complexity to the model by adding a force-based PID controller closed-loop system.

Three PCSAs (i.e., baseline, 85% of baseline, 115% of baseline), three reaction delays, and three target joint angle set values were used for the DOE. The reaction delay values were taken from relaxed muscle state experimental EMG onset times [13]. The EMG onset times from both pulse severity tests (1g and 2.5g) in the relaxed muscle state from both sides of the body were used to calculate the mean and standard deviation (SD) for each muscle. The three reaction delay values used were mean, mean - SD, and mean + SD for each body region (TABLE I). The target joint angles were changed by 10 degrees in either direction from baseline for shoulder, elbow, torso, hip, knee, and ankle joints for angles measured in the X-Z plane. For the model with muscle activation, 54 simulations were performed. The baseline model in this study represents the model with default PCSA and reaction delay values of the M50-OS+Active model, as well as the braced muscle condition target joint angles used in the previous study [2]. An additional two simulations were performed using the model without muscle activation for comparison with the active model. A total of 56 simulations were carried out in this study. The reaction forces, occupant kinematics, and peak forward excursion data were extracted from each simulation. An average CORA score was calculated for each simulation using time-history data (55 signals); the settings used for the CORA analysis were provided in the previous study [2]. To understand the effects of independent variables (i.e., PCSA, Angle, Delay) on the occupant response a multivariate linear regression analysis was carried out using peak forward excursions and average CORA score as dependent variables.

TABLE I
REACTION DELAY VALUES USED FOR THE MODELS
(MEAN ± STANDARD DEVIATION IN ms)

Body Region	M50-OS+Active
Neck	57 ± 26
Thorax	86 ± 42
Upper Extremity	53 ± 19
Pelvis	53 ± 34
Lower Extremity	63 ± 45

III. RESULTS

The peak forward excursion of various body regions for the active muscle models with three different PCSA values are compared to the experimental data and model without muscle activation in Fig. 2. Similarly, the comparison of peak forward excursion for the models with three different reaction delay values is shown in Fig. 3. The comparison of the models with three different sets of target joint angles is shown in Fig. 4. Each peak forward excursion plot contains the mean of volunteer data with one SD error bar, the results from three active models, and the results of the passive model (without muscle activation). The peak forward excursion data for all simulations with active models are reported in the appendix (Fig. A1). The peak forward excursions and average CORA scores for selected simulations of the braced 1.0g case and braced 2.5g case are reported in TABLE II and TABLE III. The ranges of forward excursions of each body region for all the experiments and simulations are reported in TABLE IV. The peak forward excursion increased with a decrease in PCSA, an increase in reaction delay, and a decrease in target joint angles (TABLE II and TABLE III). The target joint angle had the largest effect on the peak forward excursion, whereas the PCSA had the lowest effect (TABLE II and TABLE III). All the active models performed better than the passive model.

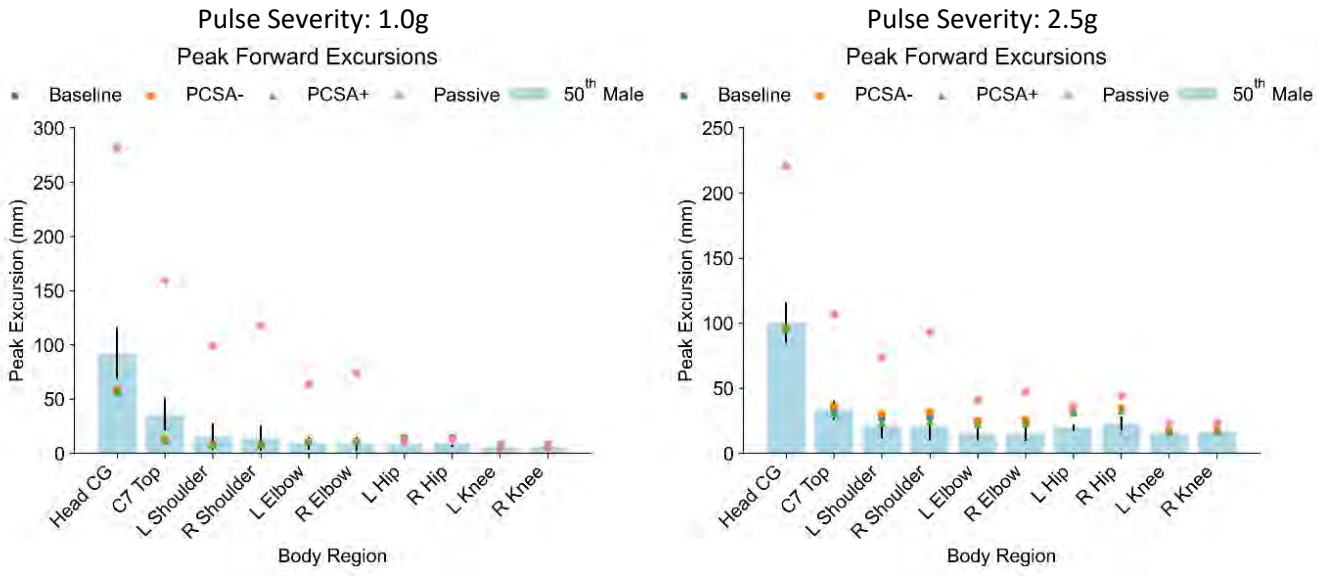

Fig. 2. Comparison of peak forward excursion of various body regions for models with three different PCSA values, model without muscle activation (Passive), and experimental data (50th Male) for pre-crash braking (1g pulse severity: left) and low-speed impact event (2.5g pulse severity: right). Baseline: default PCSA values, PCSA-: 85% of baseline PCSA values, PCSA+: 115% of baseline PCSA values, and Passive: model without muscle activation. All other variables were constant.

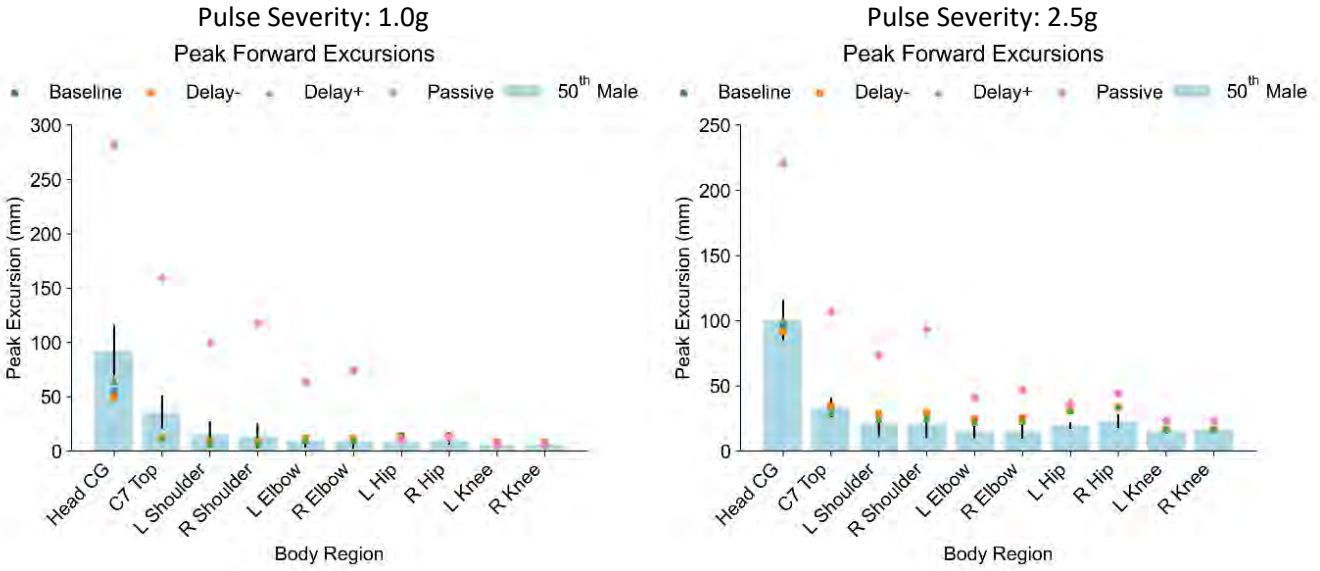

Fig. 3. Comparison of peak forward excursion of various body regions for models with three different reaction delay values, model without muscle activation (Passive), and experimental data (50th Male) for pre-crash braking (1g pulse severity: left) and low-speed impact event (2.5g pulse severity: right). Baseline: mean, Delay-: mean - SD, Delay+: mean + SD (TABLE I), and Passive: model without muscle activation. All other variables were constant.

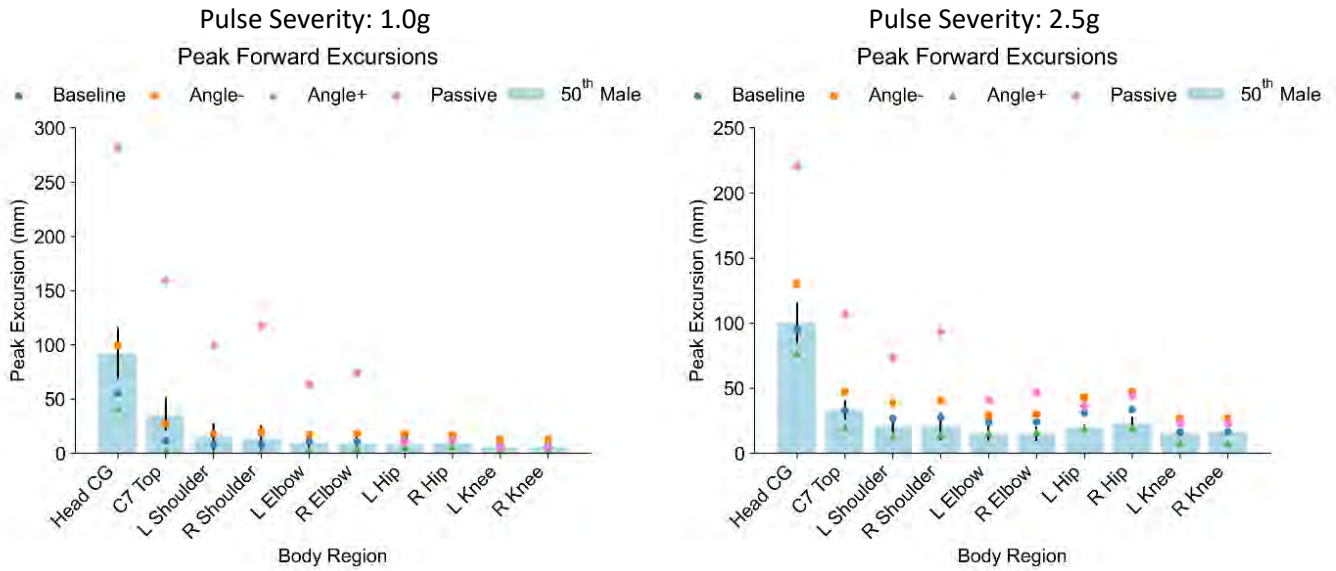

Fig. 4. Comparison of peak forward excursion of various body regions for models with three different target joint angle values, model without muscle activation (Passive), and experimental data (50th Male) for pre-crash braking (1g pulse severity: left) and low-speed impact event (2.5g pulse severity: right). Baseline: default values, Angle-: baseline – 10 degrees, Angle+: mean + 10 degrees, and Passive: model without muscle activation. All other variables were constant.

The comparison of reaction forces and the belt forces for active models with three different target joint angle values, the passive model, and the experimental data are reported in Fig. 5 - Fig. 11, and all active model simulations are compared in Fig. A2 - Fig. A8. The reaction forces increased with an increase in target joint angles whereas belt forces decreased initially but increased later (Fig. 10 and Fig. 11). Due to the larger error between the measured and target joint angles, the muscle forces were higher, leading to increased reaction forces. As a result, the model came off the seat pan later in the simulation, loading the lap belt as the simulation progressed. Similar observations were made for PCSA. No considerable changes were observed in forces with changes in reaction delay. The range of average CORA scores for all the simulations is provided in TABLE IV. All the time-history plots used in the CORA analysis are provided in the Fig. A2- Fig. A 56. These figures include time-history data for X, Y, and Z displacement and acceleration of various body markers along with reaction forces.

TABLE II
FORWARD EXCURSION OF VARIOUS BODY REGIONS AND AVERAGE CORA SCORE FOR SELECTED SIMULATIONS FOR 1.0G CASE

Variable	Experiment	Baseline	PCSA-	PCSA+	Delay-	Delay+	Angle-	Angle+
Head CG Forward Excursion (mm)	92 ± 23	55.4	58.5	56.9	49.8	64.4	99.2	40.7
C7 Top Forward Excursion (mm)	36 ± 14	11.7	12.6	11.4	11.3	11.3	26.7	2.7
L Shoulder Forward Excursion (mm)	15 ± 12	8.1	7.7	7.9	8.4	7.1	17.8	0.0
R Shoulder Forward Excursion (mm)	13 ± 11	8.2	8.2	8.2	8.4	7.4	19.3	0.4
L Elbow Forward Excursion (mm)	9 ± 5	10.9	10.6	11.0	11.3	10.2	17.4	3.1
R Elbow Forward Excursion (mm)	8 ± 6	10.9	10.9	11.3	11.1	10.4	18.1	3.8
L Hip Forward Excursion (mm)	7 ± 2	14.5	13.8	14.7	14.5	14.4	18.1	5.5
R Hip Forward Excursion (mm)	9 ± 3	14.4	13.4	14.4	14.3	14.4	17.1	6.3
L Knee Forward Excursion (mm)	5 ± 1	8.2	7.4	8.9	8.2	8.1	12.3	1.7
R Knee Forward Excursion (mm)	5 ± 1	8.2	7.4	8.9	8.2	8.1	12.3	1.7
Average CORA Score	-	0.48	0.51	0.48	0.48	0.49	0.47	0.41

TABLE III
FORWARD EXCURSION OF VARIOUS BODY REGIONS AND AVERAGE CORA SCORE FOR SELECTED SIMULATIONS FOR 2.5G CASE

Variable	Experiment	Baseline	PCSA-	PCSA+	Delay-	Delay+	Angle-	Angle+
Head CG Forward Excursion (mm)	100 ± 15	95.4	96.4	96.1	91.8	99.9	130.4	76.4
C7 Top Forward Excursion (mm)	33 ± 7	32.9	36.2	30.1	34.6	30.0	47.0	19.6
L Shoulder Forward Excursion (mm)	20 ± 8	26.6	30.1	23.1	28.2	24.4	38.7	13.8
R Shoulder Forward Excursion (mm)	20 ± 10	27.6	31.5	24.2	29.1	25.5	40.2	14.5
L Elbow Forward Excursion (mm)	15 ± 5	23.7	24.9	22.2	24.8	22.0	28.9	15.5
R Elbow Forward Excursion (mm)	15 ± 5	24.2	25.6	22.9	25.1	22.9	29.9	16.3
L Hip Forward Excursion (mm)	19 ± 2	31.2	32.1	30.9	31.0	31.4	42.9	18.8
R Hip Forward Excursion (mm)	22 ± 5	33.7	34.1	32.8	33.4	33.9	47.4	19.5
L Knee Forward Excursion (mm)	15 ± 2	16.7	17.3	16.5	16.5	16.8	27.2	7.8
R Knee Forward Excursion (mm)	16 ± 2	16.7	17.3	16.5	16.5	16.8	27.2	7.8
Average CORA Score	-	0.49	0.48	0.49	0.49	0.49	0.40	0.56

TABLE IV
RANGE OF FORWARD EXCURSION OF VARIOUS BODY REGIONS AND AVERAGE CORA SCORE FOR ALL THE SIMULATIONS OF THE DOE

Variable	Braced 1.0g		Braced 2.5 g	
	Experiment	Simulation	Experiment	Simulation
Head CG Forward Excursion (mm)	92 ± 23	66 ± 26	100 ± 15	101 ± 23
C7 Top Forward Excursion (mm)	36 ± 14	13 ± 10	33 ± 7	33 ± 11
L Shoulder Forward Excursion (mm)	15 ± 12	8 ± 7	20 ± 8	26 ± 10
R Shoulder Forward Excursion (mm)	13 ± 11	9 ± 8	20 ± 10	27 ± 11
L Elbow Forward Excursion (mm)	9 ± 5	10 ± 6	15 ± 5	22 ± 5
R Elbow Forward Excursion (mm)	8 ± 6	11 ± 6	15 ± 5	23 ± 5
L Hip Forward Excursion (mm)	7 ± 2	12 ± 5	19 ± 2	30 ± 9
R Hip Forward Excursion (mm)	9 ± 3	12 ± 4	22 ± 5	33 ± 11
L Knee Forward Excursion (mm)	5 ± 1	7 ± 4	15 ± 2	17 ± 7
R Knee Forward Excursion (mm)	5 ± 1	7 ± 4	16 ± 2	17 ± 7
Average CORA Score	-	0.45 ± 0.04	-	0.49 ± 0.06

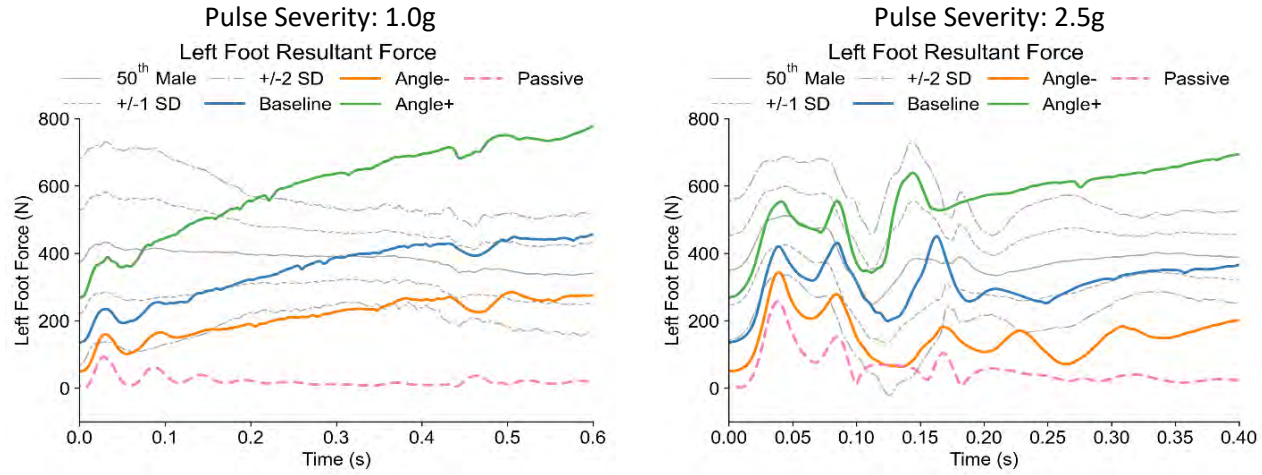

Fig. 5. Comparison of Left Foot Resultant Force for models with three different target joint angle values, model without muscle activation (Passive), and experimental data (50th Male) for pre-crash braking (1g pulse severity: left) and low-speed impact event (2.5g pulse severity: right). Baseline: default values, Angle-: baseline – 10 degrees, Angle+: mean + 10 degrees, and Passive: model without muscle activation. All other variables were constant.

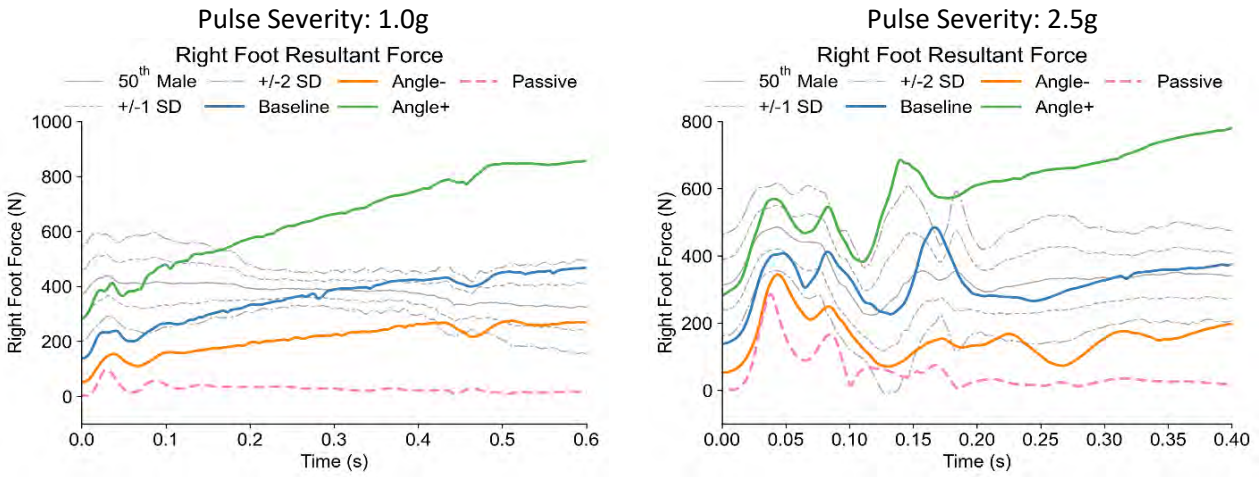

Fig. 6. Comparison of Right Foot Resultant Force for models with three different target joint angle values, model without muscle activation (Passive), and experimental data (50th Male) for pre-crash braking (1g pulse severity: left) and low-speed impact event (2.5g pulse severity: right). Baseline: default values, Angle-: baseline – 10 degrees, Angle+: mean + 10 degrees, and Passive: model without muscle activation. All other variables were constant.

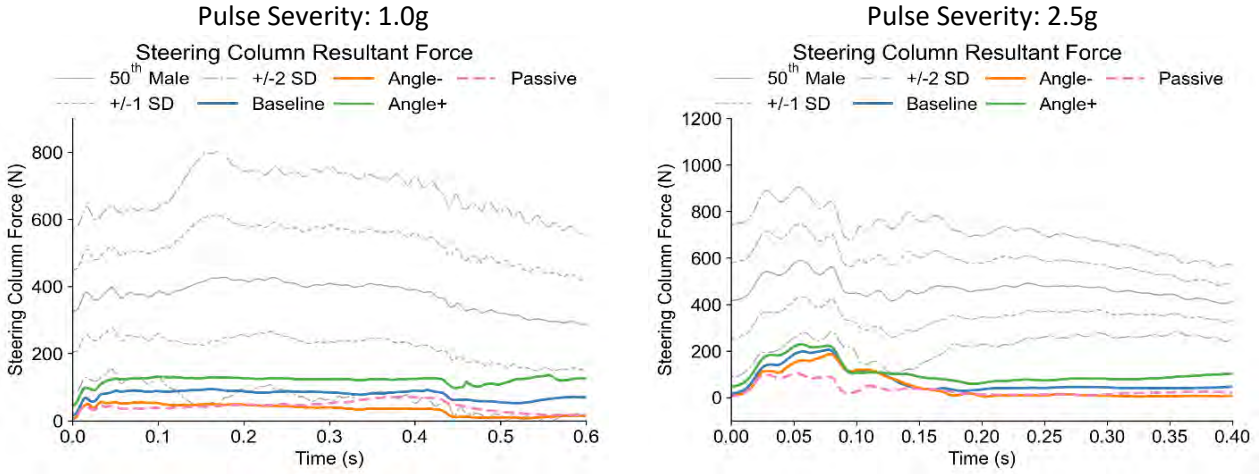

Fig. 7. Comparison of Steering Column Resultant Force for models with three different target joint angle values, model without muscle activation (Passive), and experimental data (50th Male) for pre-crash braking (1g pulse severity: left) and low-speed impact event (2.5g pulse severity: right). Baseline: default values, Angle-: baseline – 10 degrees, Angle+: mean + 10 degrees, and Passive: model without muscle activation. All other variables were constant.

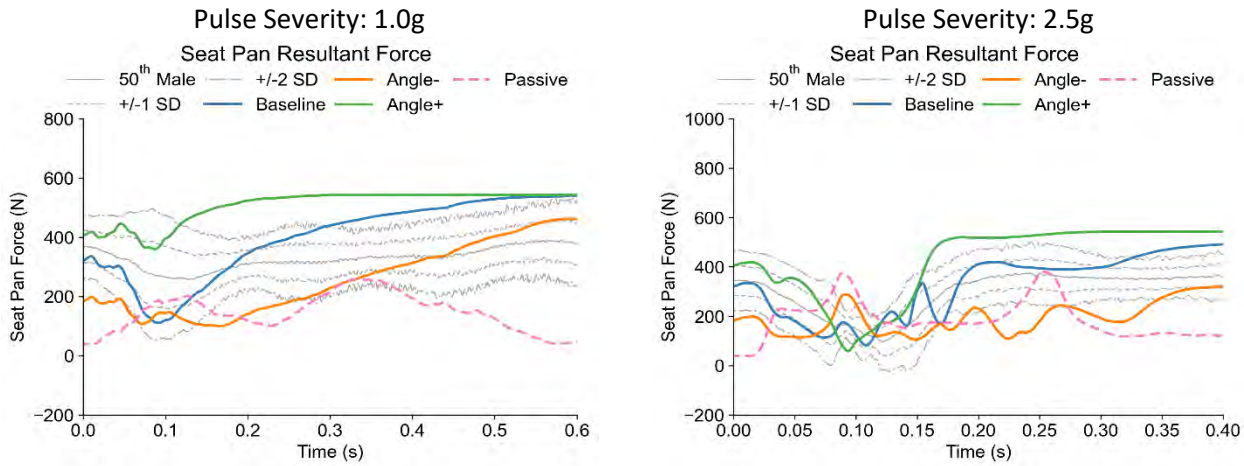

Fig. 8. Comparison of Seat Pan Resultant Force for models with three different target joint angle values, model without muscle activation (Passive), and experimental data (50th Male) for pre-crash braking (1g pulse severity: left) and low-speed impact event (2.5g pulse severity: right). Baseline: default values, Angle-: baseline – 10 degrees, Angle+: mean + 10 degrees, and Passive: model without muscle activation. All other variables were constant.

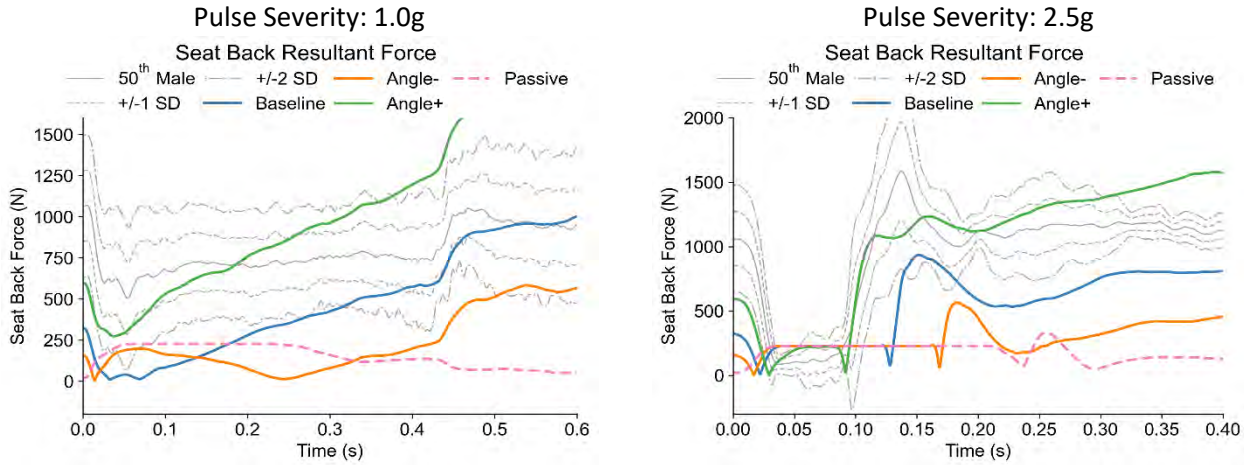

Fig. 9. Comparison of Seat Back Resultant Force for models with three different target joint angle values, model without muscle activation (Passive), and experimental data (50th Male) for pre-crash braking (1g pulse severity: left) and low-speed impact event (2.5g pulse severity: right). Baseline: default values, Angle-: baseline – 10 degrees, Angle+: mean + 10 degrees, and Passive: model without muscle activation. All other variables were constant.

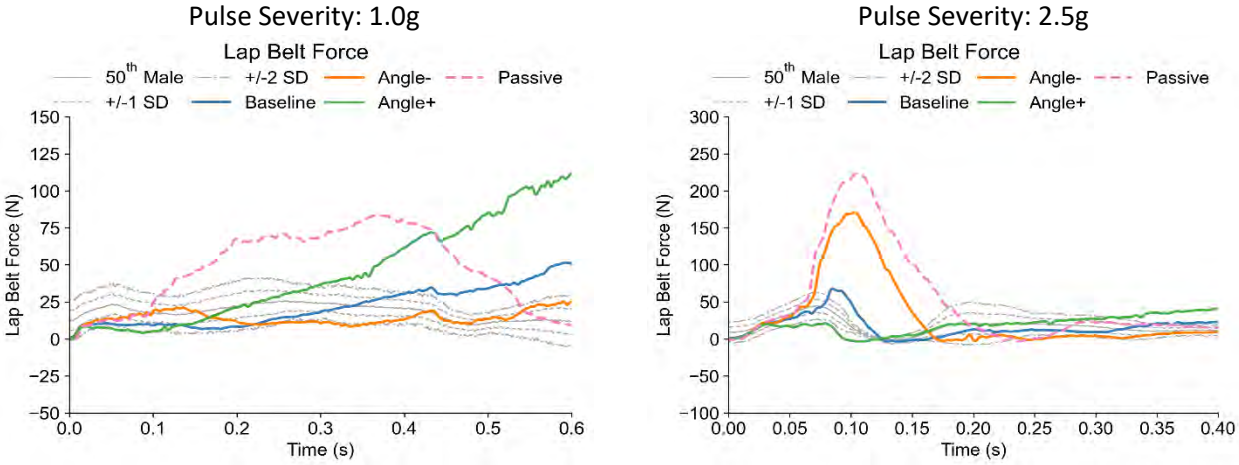

Fig. 10. Comparison of Lap Belt Force for models with three different target joint angle values, model without muscle activation (Passive), and experimental data (50th Male) for pre-crash braking (1g pulse severity: left) and low-speed impact event (2.5g pulse severity: right). Baseline: default values, Angle-: baseline – 10 degrees, Angle+: mean + 10 degrees, and Passive: model without muscle activation. All other variables were constant.

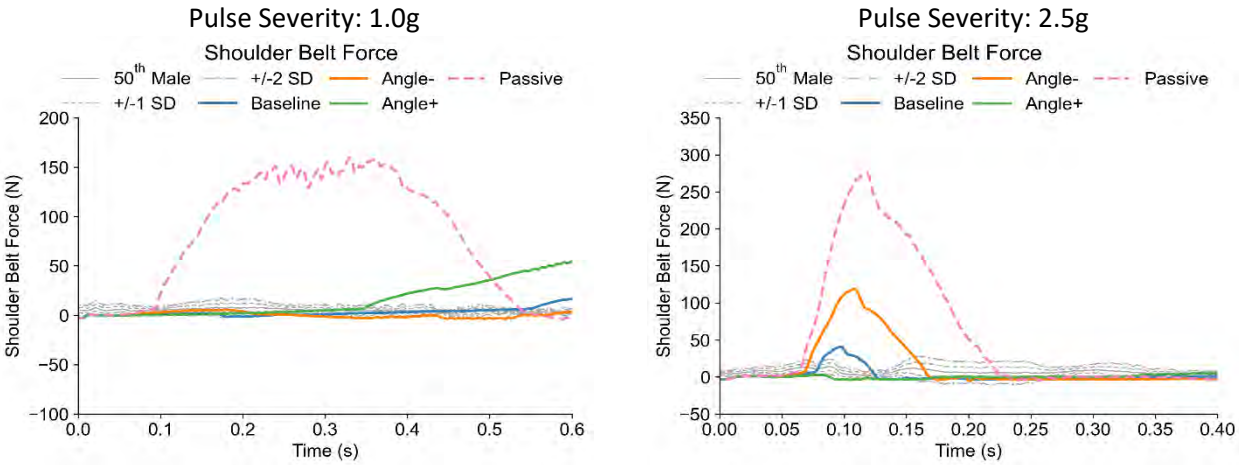

Fig. 11. Comparison of Shoulder Belt Force for models with three different target joint angle values, model without muscle activation (Passive), and experimental data (50th Male) for pre-crash braking (1g pulse severity: left) and low-speed impact event (2.5g pulse severity: right). Baseline: default values, Angle-: baseline – 10 degrees, Angle+: mean + 10 degrees, and Passive: model without muscle activation. All other variables were constant.

The results of the multivariate linear regression model that was fit using PCSA, target joint angle (Angle), and reaction delay (Delay) as categorical independent variables and all the peak forward excursions for different body regions as shown in Fig. 2 - Fig. 4 and CORA score as dependent variables are shown in Fig. 12 and Fig. A57 - Fig. A66 in the appendix. Each of these plots has three subplots for each independent variable and two bars representing the coefficients of each categorical value relative to the baseline of each variable. If the coefficients were statistically significant ($p<0.05$) an "*" was added to the X-axis label. A positive coefficient value represents an increase in the dependent variable value relative to the baseline in that category and a negative coefficient represents a decrease. The CORA scores decreased for both pulse severities with a decrease in target joint angles. They decreased for 1.0g pulse severity and increased for 2.5g pulse severity when target joint angles were increased (Fig. 12). All the peak forward excursions increased with a decrease in target joint angles and increased with an increase in target joint angles (Fig. A57 - Fig. A66). The effect of target joint angles on the CORA score and peak forward excursion was statistically significant.

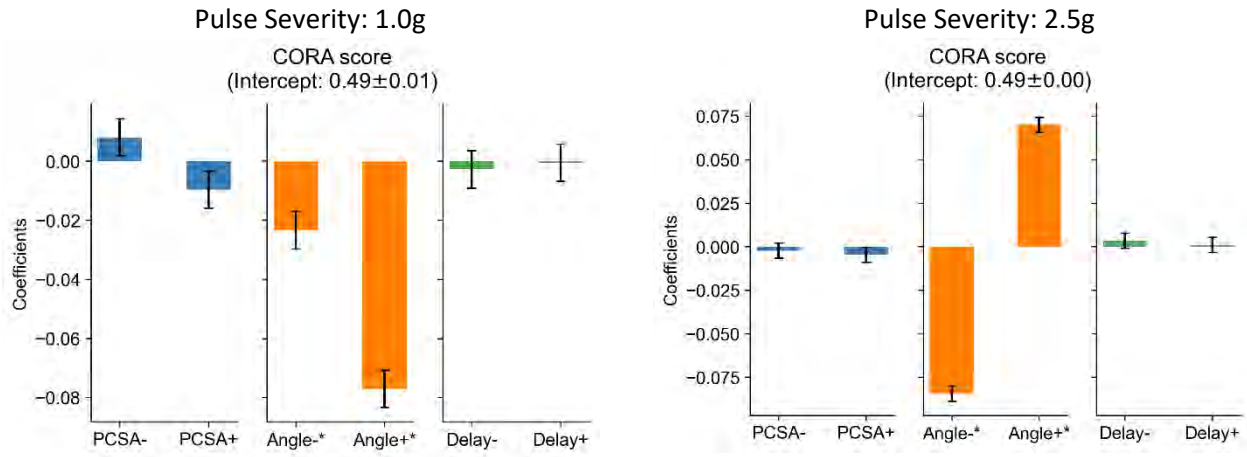

Fig. 12. Results of multivariate linear regression analysis for CORA score for pre-crash braking (1g pulse severity: left) and low-speed impact event (2.5g pulse severity: right). Each subplot represents one independent variable category, each bar represents coefficients from the linear model, and the error bars show standard error. The coefficients are relative to the reference level in each category i.e. baseline value. X-ticks have * for statistically significant results.

IV. DISCUSSION

The objective of the study was to assess the ability of AHBMs to capture the variability in occupant bracing and this was carried out by varying the three parameters of the AHBM (i.e., PCSA, target joint angles, and reaction delay) that are directly related to the muscle forces generated by the model. There are very few studies that have simulated braced muscle conditions using AHBMS [2,3,15,23,24,26]. Meijer et al. [26] has used 30% co-contraction for neck and arm muscles along with setting activation parameters to 1 for all body regions to simulate braced muscle condition, whereas Chancey et al. [15] activated neck muscles pre-impact to simulate neck bracing. However, none of the studies has looked at various methods to simulate various bracing levels and their effects on occupant kinematics. This is the first time a study has investigated different ways of modeling occupant bracing and the subsequent effects on occupant kinetics and kinematics.

The reaction forces at the contact surfaces increased (Fig. 5- Fig. 9) and peak forward excursion decreased (Fig. A57 - Fig. A66) with an increase in target joint angles. Similarly, reaction forces increased with an increase in PCSA, and no significant changes to the reaction forces were observed with changes in reaction delay. Three clusters were observed in the reaction force time-history data from all the simulations of the DOE which were far apart from each other due to three target joint angles. Each cluster had three sets of curves due to three PCSA values, and there were three curves on top of each other due to differences in the reaction delay (Fig. A2 - Fig. A6). The PCSA and reaction delay had mixed effects on peak forward excursion data and not all of the results were statistically significant (Fig. A57 - Fig. A66). In a study by Lalwala et al. [27], a modular spine version of the M50-OS+Active model was used to study the sensitivity of loading conditions, PCSA, and reaction time on astronaut response for a relaxed subject. The authors also reported the minimal effect of PCSA and reaction time on the model performance.

The spread of peak forward excursions observed from all the simulations was mostly within the experimental corridors, but not all of the time history plots are within experimental corridors, which is reflected in the CORA scores. Based on the average CORA score of selected simulations where only one parameter was varied, Angle+ had the worst (0.41) response in the braced 1.0g case and the best (0.56) response in 2.5g pulse severity. This suggests that increasing the target joint angles will improve the performance of the model in the 2.5g case but worsen the response in the 1.0g case. However, there were still several combinations of PCSA, target joint angle, and delay parameters that had better CORA scores and peak forward excursion data that fell within the experimental corridors. The maximum value of the CORA score was 0.57, which seems very low and raises questions about the bifidelity of the models and the use of CORA analysis for model assessment. This study used a set of 55 time-history signals to calculate the average CORA score for each simulation, including reaction forces, displacements, and acceleration data. Considering the number of traces used, it is not uncommon to get low CORA scores. Very few studies have used CORA with this many time-history data points. Usually, researchers compare data of a specific body region, or if using x, y, and z components of a signal, they apply weighting based

on the direction that closely aligns with the loading direction. No such strategies were employed in this study.

There are some limitations of this study. The study was not able to reproduce the different trends in the pre-test bracing that were reported by Albert et al. [18] using foot pedal force time-history data. The model only had 300 ms before the start of the pulse to brace itself against the contacting surfaces and within that period only "Peak before steady-state" trends were observed. The peak before a steady-state trend is where the bracing force reaches a peak and then experiences a brief period of decrease followed by a sustained constant force until the sled pulse starts. This was probably due to the use of higher joint angles to simulate occupant bracing. It is also not computationally cost-effective to use a model to simulate bracing for a longer period before the start of the pulse. Another limitation of the study is that only one model was used and that represents mid-size males due to the availability of experimental volunteer data for same-body habitus. In future studies, a similar approach can be carried out with the 5th percentile female volunteer data that were collected by Chan et al. [13]. Future studies with models of different sizes and sexes will be useful to capture the variation in a mixed population instead of the single model used in this study to capture variation in a single set of volunteers representing one body habitus. Finally, this study used data from only low-speed frontal sled tests. It will be interesting to look at model responses in other impact directions.

V. CONCLUSIONS

The current study used an AHBM representing a mid-size male and was able to capture the variability in the occupant bracing and kinematics of five volunteers by varying PCSA, reaction delay, and target joint angles. This study looked at the effect size using a multivariate linear regression model that was fit between three independent variables (PCSA, Angle, and Delay) and 11 dependent variables (peak forward excursions and CORA score). The target joint angles had the largest effect on occupant response and were statistically significant followed by PCSA and reaction delay. Not all the peak forward excursions and CORA scores were significantly affected by PCSA and reaction delay. The results of the study suggest that the variability in occupant bracing can be captured by one AHBM and be used to study the effect of bracing on occupant response in future studies.

VI. ACKNOWLEDGEMENTS

Work was supported by the Global Human Body Models Consortium, LLC, and NHTSA under GHBMC Project No.: WFU-006. All simulations were run on the DEAC cluster at Wake Forest University with support from Stevens Cody and Adam Carlson.

VII. DISCLOSURE STATEMENT

F. Scott Gayzik is a member of Elemance, LLC., which distributes academic and commercial licenses for the use of GHBMC-owned computational human body models.

VIII. REFERENCES

[1] Devane, K., Chan, H., Albert, D., Kemper, A., and Gayzik, F.S. Implementation and calibration of active small female and average male human body models using low-speed frontal sled tests. *Traffic Injury Prevention*, 2022. 23(sup1): p. S44-S49

[2] Devane, K., Chan, H., Albert, D., Kemper, A., and Gayzik, F.S. Response of small female and midsize male models with active musculature in pre-crash maneuvers and low-speed impacts. *Traffic Inj Prev*, 2023. 24(sup1): p. S9-S15

[3] Kato, D., Nakahira, Y., and Iwamoto, M. A study of muscle control with two feedback controls for posture and reaction force for more accurate prediction of occupant kinematics in low-speed frontal impacts. *Proceedings of 25th International Technical Conference on the Enhanced Safety of Vehicles (ESV) National Highway Traffic Safety Administration*, 2017. Detroit, Michigan USA

[4] Diederich, A., Bastien, C., Ekambaram, K., and Wilson, A. Occupant pre-crash kinematics in rotated seat arrangements. *Proceedings of the Institution of Mechanical Engineers, Part D: Journal of Automobile Engineering*, 2021

[5] Mishra, E. and Lubbe, N. Assessing injury risks of reclined occupants in a frontal crash preceded by braking with varied seatbelt designs using the SAFER Human Body Model. *Traffic Injury Prevention*, 2024. 25(3): p. 445-453

[6] Osth, J., Brolin, K., and Brase, D. A human body model with active muscles for simulation of pretensioned restraints in autonomous braking interventions. *Traffic Inj Prev*, 2015. 16: p. 304-13
[7] Boyle, K., Fanta, A., et al. Restraint systems considering occupant diversity and pre-crash posture. *Traffic Injury Prevention*, 2020. 21(sup1): p. S31-S36
[8] Ejima, S., Zama, Y., et al. Prediction of the physical motion of the human body based on muscle activity during pre-impact braking. *Proceedings of Proceedings of the IRCOBI Conference*, 2008. Bern, Switzerland
[9] Osth, J., Olafsdottir, J.M., Davidsson, J., and Brolin, K. Driver kinematic and muscle responses in braking events with standard and reversible pre-tensioned restraints: validation data for human models. *Stapp Car Crash J*, 2013. 57: p. 1-41
[10] Nie, B., Sathyanarayan, D., Ye, X., Crandall, J.R., and Panzer, M.B. Active muscle response contributes to increased injury risk of lower extremity in occupant–knee airbag interaction. *Traffic injury prevention*, 2018. 19(sup1): p. S76-S82
[11] Putra, I.P.A., Carmai, J., Koetniyom, S., and Markert, B. The Effects of Active Muscle Contraction into Pedestrian Kinematics and Injury during Vehicle-Pedestrian Collision. *Proceedings of 10th european ls-dyna conference*, 2015. Würzburg, Germany
[12] Beeman, S.M., Kemper, A.R., Madigan, M.L., and Duma, S.M. Effects of bracing on human kinematics in low-speed frontal sled tests. *Ann Biomed Eng*, 2011. 39(12): p. 2998-3010
[13] Chan, H., Albert, D.L., Gayzik, F.S., and Kemper, A.R. Occupant Kinetics and Muscle Responses of Relaxed and Braced Small Female and Mid-Size Male Volunteers in Low-Speed Frontal Sled Tests. *SAE International Journal of Transportation Safety*, 2023
[14] Chan, H., Albert, D.L., Gayzik, F.S., and Kemper, A.R. Occupant Kinematics of Braced 5th Percentile Female and 50th Percentile Male Volunteers in Low-Speed Frontal and Frontal-Oblique Sled Tests, in *IRCOBI*. 2022: Porto, Portugal.
[15] Chancey, V.C., Nightingale, R.W., Van Ee, C.A., Knaub, K.E., and Myers, B.S. Improved estimation of human neck tensile tolerance: reducing the range of reported tolerance using anthropometrically correct muscles and optimized physiologic initial conditions. *Stapp Car Crash J*, 2003. 47: p. 135-53
[16] Cutcliffe, H., Brolin, K., Östh, J., Ólafsdóttir, J.M., and Davidsson, J. Gender Differences in Occupant Posture and Muscle Activity with Motorized Seat Belts. *Proceedings of The 24th ESV Conference Proceedings*, 2015. Gothenburg, Sweden
[17] Ejima, S., Ono, K., Holcombe, S., Kaneoka, K., and Fukushima, M. A study on occupant kinematics behaviour and muscle activities during pre-impact braking based on volunteer tests. *Proceedings of Proceedings of ircobi (international research council on the biomechanics of injury) conference 2007, held maastricht, the netherlands, september 2007*, 2007.
[18] Albert, D., Chan, H., Gayzik, F.S., and Kemper, A. Volunteer Bracing Strategies and Variability before Low-Speed Frontal and Frontal-Oblique Sled Tests. *Proceedings of International Research Council on the Biomechanics of Injury Conference*, 2023. Cambridge, United Kingdom
[19] Devane, K., Hsu, F.-C., et al. Assessment of finite element human body and ATD models in estimating injury risk in far-side impacts using field-based injury risk. *Accident Analysis & Prevention*, 2023. 192
[20] Decker, W.B., Jones, D.A., et al. Effect of body size and enhanced helmet systems on risk for motorsport drivers. *Traffic Injury Prevention*, 2021. 22(sup1): p. S49-S55
[21] Chan, H., Albert, D.L., Gayzik, F.S., and Kemper, A.R. Assessment of acclimation of 5th percentile female and 50th percentile male volunteer kinematics in low-speed frontal and frontal-oblique sled tests. *SAE International journal of transportation safety*, 2021. 9(1): p. 3-103
[22] Chan, H., Devane, K.S., Albert, D.L., Gayzik, F.S., and Kemper, A.R. Comparisons of Initial Joint Angles and Test Buck Reaction Forces for Relaxed and Braced 5th Percentile Female and 50th Percentile Male Volunteers and Analogous Active Human Body Models in a Simulated Driver's Seat, in *IRCOBI*. 2021: Online.
[23] Devane, K., Johnson, D., and Gayzik, F.S. Validation of a simplified human body model in relaxed and braced conditions in low-speed frontal sled tests. *Traffic Injury Prevention*, 2019. 20(8): p. 832-837
[24] Devane, K. and Gayzik, F.S. A simulation-based study for optimizing proportional-integral-derivative controller gains for different control strategies of an active upper extremity model using experimental data. *Computer Methods in Biomechanics and Biomedical Engineering*, 2023: p. 1-14

[25] Olafsdottir, J.M., Östh, J., Davidsson, J., and Brolin, K. Passenger kinematics and muscle responses in autonomous braking events with standard and reversible pre-tensioned restraints. *Proceedings of International Research Council on Biomechanics of Injury*, 2013. Gothenburg, Sweden

[26] Meijer, M., Broos, J., et al. Modelling of bracing in a multi-body active human model. *Proceedings of International Research Council on Biomechanics of Injury*, 2013. Gothenburg, Sweden

[27] Lalwala, M., Devane, K.S., et al. Sensitivity Analysis for Multidirectional Spaceflight Loading and Muscle Deconditioning on Astronaut Response. *Annals of Biomedical Engineering*, 2022

IX. APPENDIX

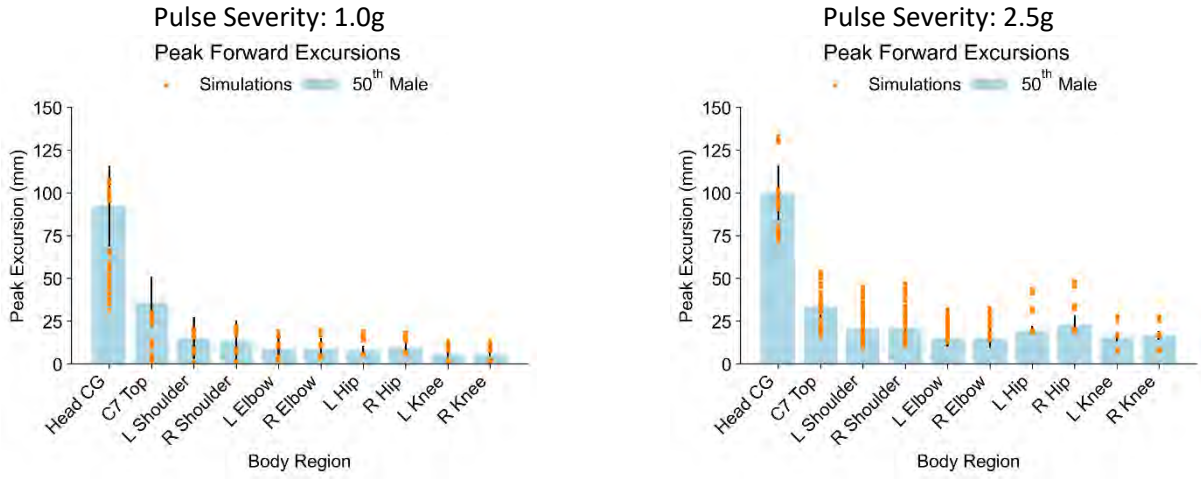

Fig. A1. Comparison of peak forward excursion of various body regions for all simulations with active muscles and experimental data (50th Male) for pre-crash braking (1g pulse severity: left) and low-speed impact event (2.5g pulse severity: right).

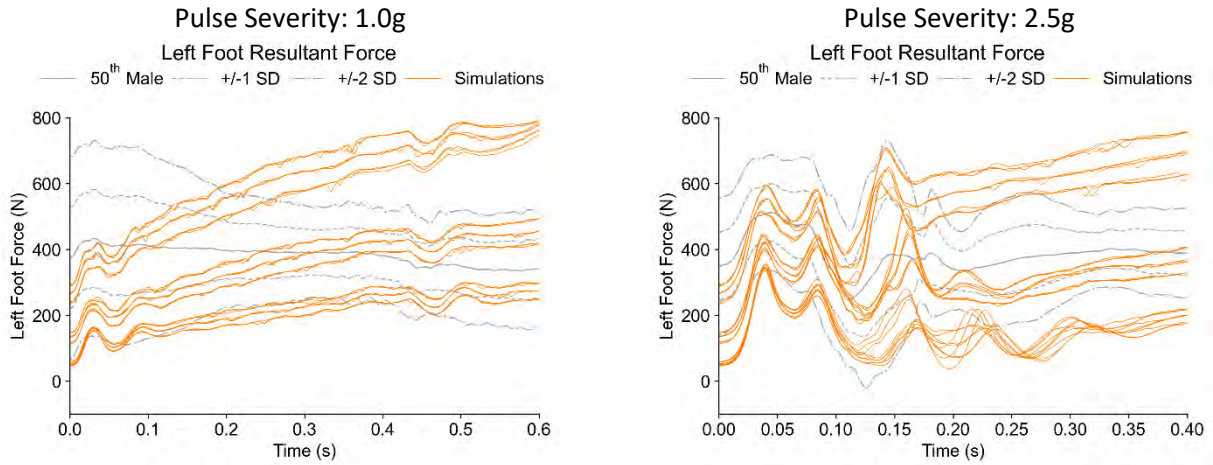

Fig. A2. Comparison of Left Foot Resultant Force for all simulations with active muscles and experimental data (50th Male) for pre-crash braking (1g pulse severity: left) and low-speed impact event (2.5g pulse severity: right).

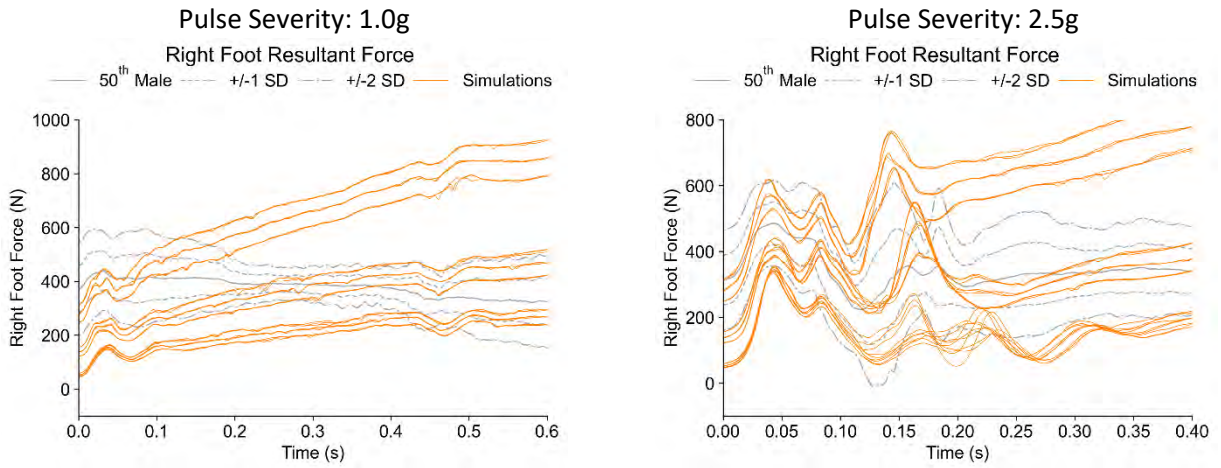

Fig. A3. Comparison of Right Foot Resultant Force for all simulations with active muscles and experimental data (50th Male) for pre-crash braking (1g pulse severity: left) and low-speed impact event (2.5g pulse severity: right).

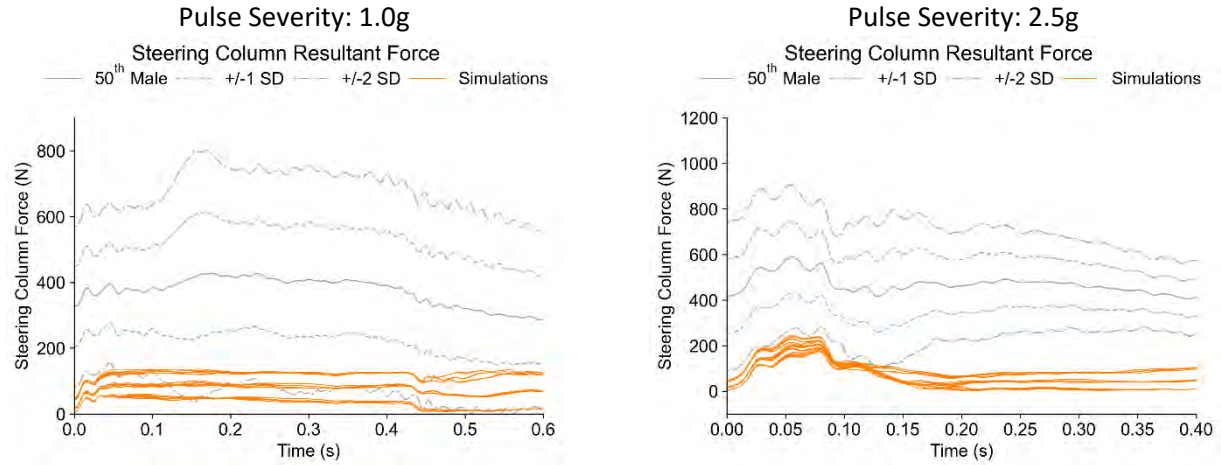

Fig. A4. Comparison of Steering Column Resultant Force for all simulations with active muscles and experimental data (50th Male) for pre-crash braking (1g pulse severity: left) and low-speed impact event (2.5g pulse severity: right).

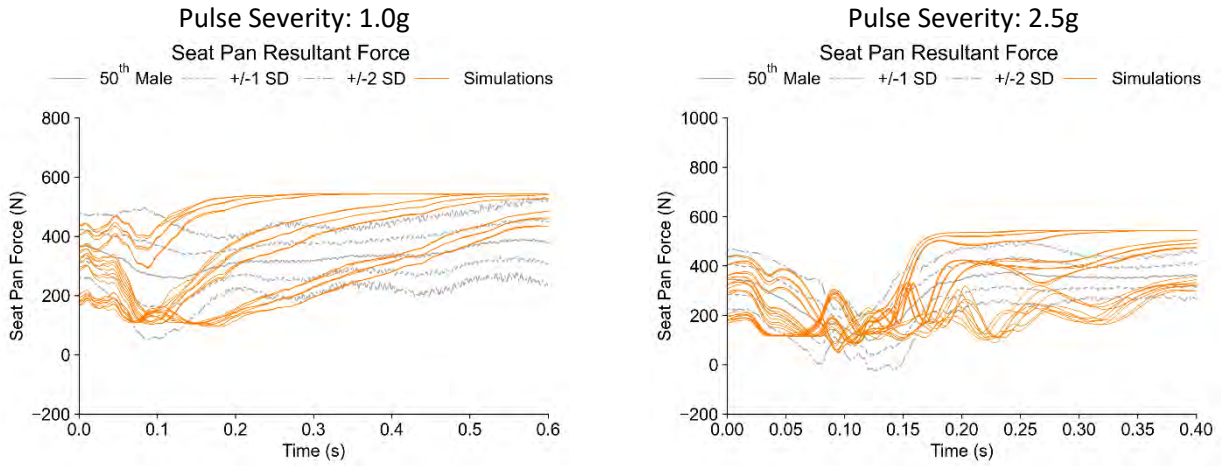

Fig. A5. Comparison of Seat Pan Resultant Force for all simulations with active muscles and experimental data (50th Male) for pre-crash braking (1g pulse severity: left) and low-speed impact event (2.5g pulse severity: right).

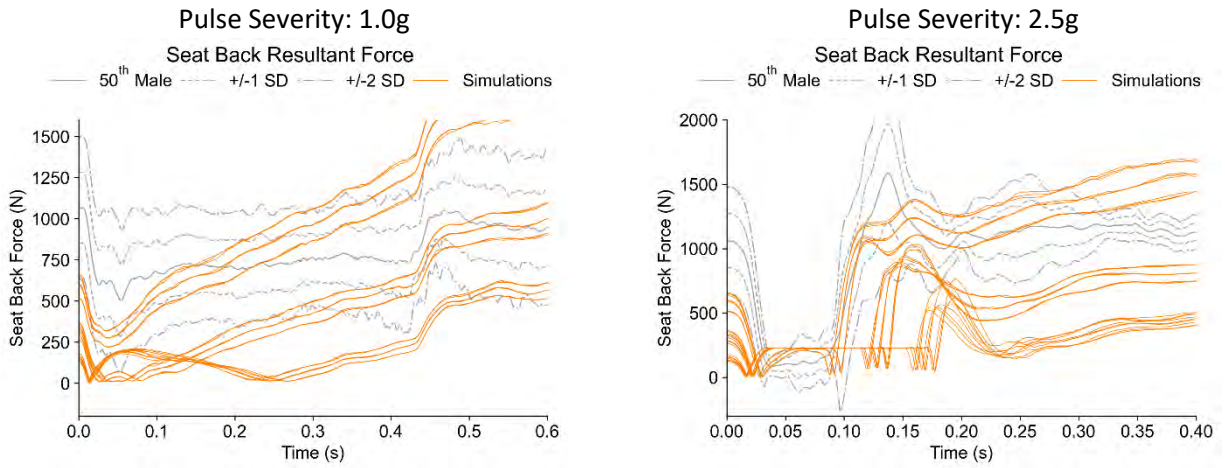

Fig. A6. Comparison of Seat Back Resultant Force for all simulations with active muscles and experimental data (50th Male) for pre-crash braking (1g pulse severity: left) and low-speed impact event (2.5g pulse severity: right).

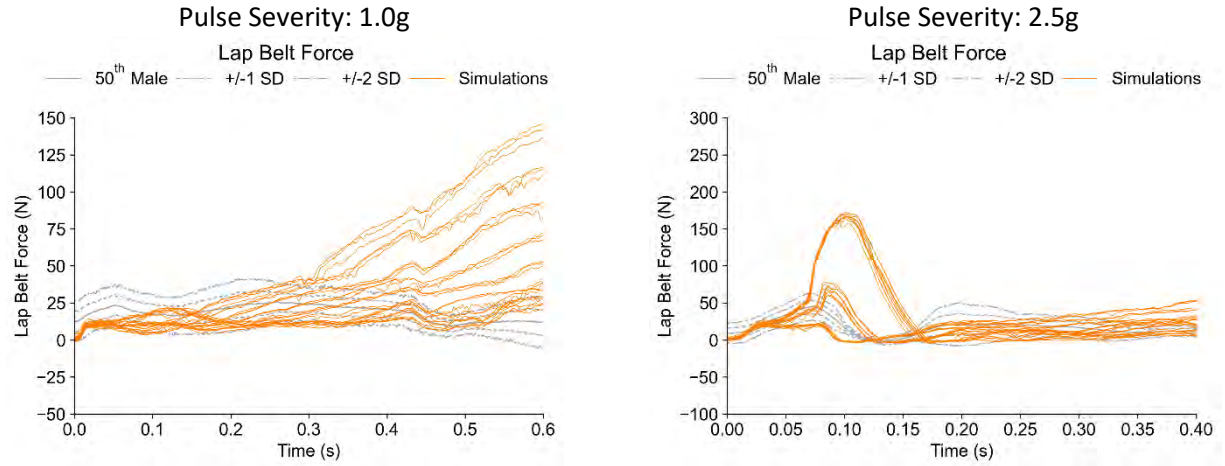

Fig. A7. Comparison of Lap Belt Force for all simulations with active muscles and experimental data (50th Male) for pre-crash braking (1g pulse severity: left) and low-speed impact event (2.5g pulse severity: right).

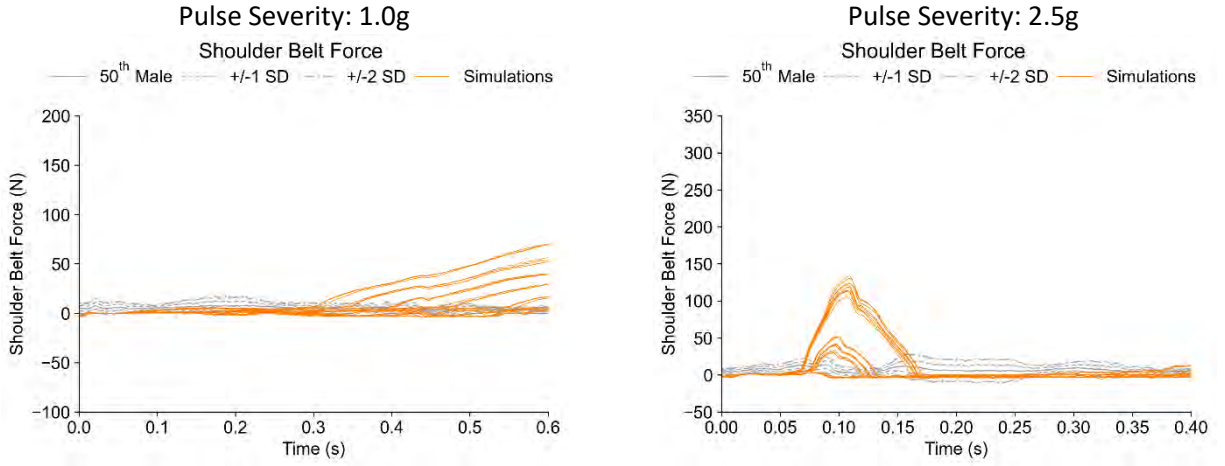

Fig. A8. Comparison of Shoulder Belt Force for all simulations with active muscles and experimental data (50th Male) for pre-crash braking (1g pulse severity: left) and low-speed impact event (2.5g pulse severity: right).

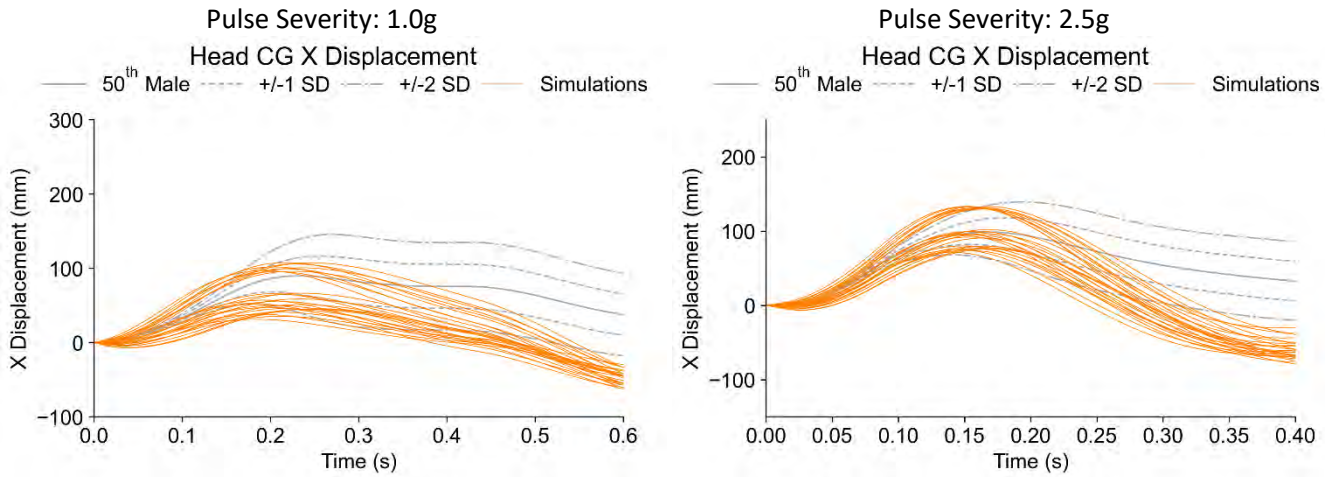

Fig. A 9. Comparison of Head CG X Displacement for all simulations with active muscles and experimental data (50th Male) for pre-crash braking (1g pulse severity: left) and low-speed impact event (2.5g pulse severity: right).

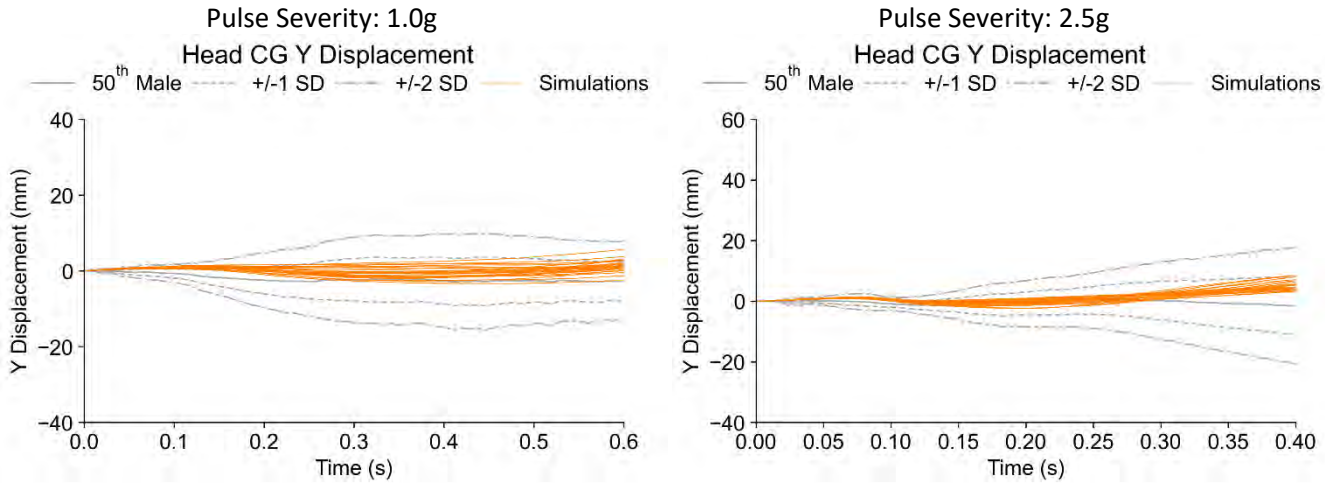

Fig. A 10. Comparison of Head CG Y Displacement for all simulations with active muscles and experimental data (50th Male) for pre-crash braking (1g pulse severity: left) and low-speed impact event (2.5g pulse severity: right).

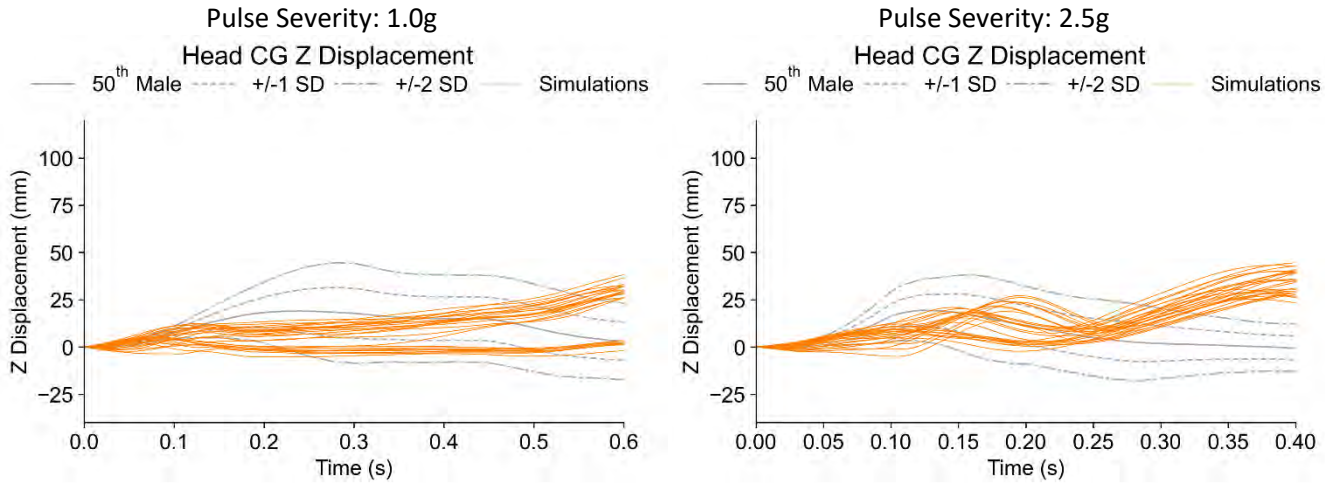

Fig. A 11. Comparison of Head CG Z Displacement for all simulations with active muscles and experimental data (50th Male) for pre-crash braking (1g pulse severity: left) and low-speed impact event (2.5g pulse severity: right).

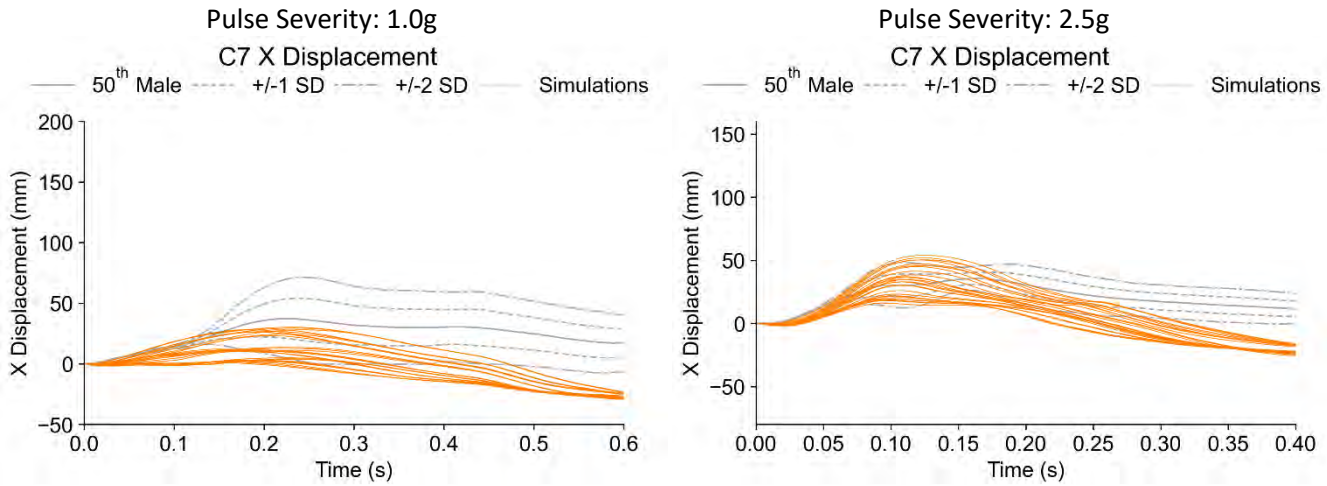

Fig. A 12. Comparison of C7 X Displacement for all simulations with active muscles and experimental data (50th Male) for pre-crash braking (1g pulse severity: left) and low-speed impact event (2.5g pulse severity: right).

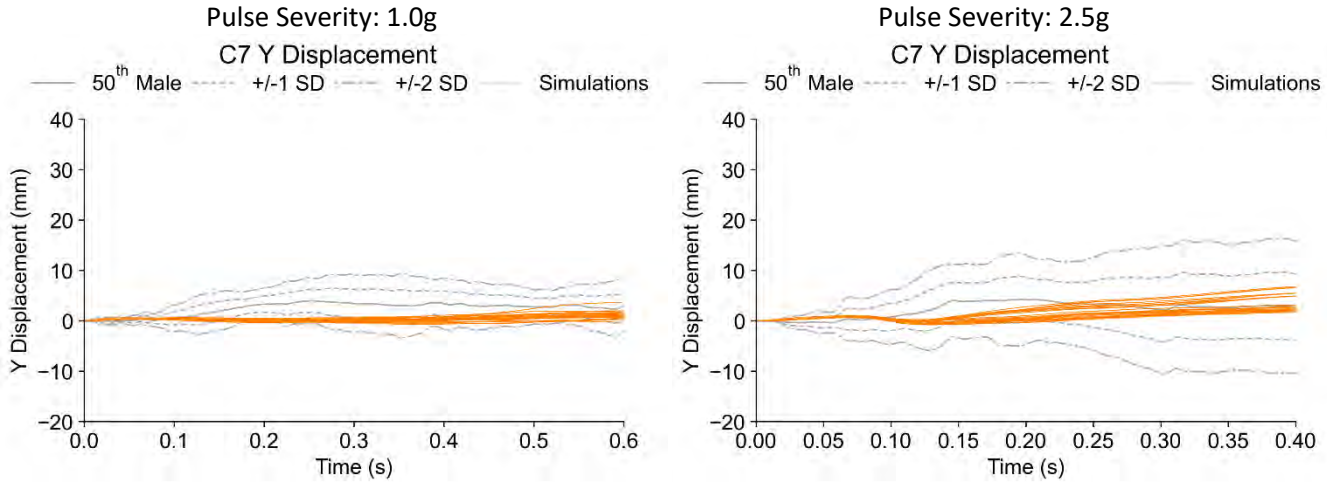

Fig. A 13. Comparison of C7 Y Displacement for all simulations with active muscles and experimental data (50th Male) for pre-crash braking (1g pulse severity: left) and low-speed impact event (2.5g pulse severity: right).

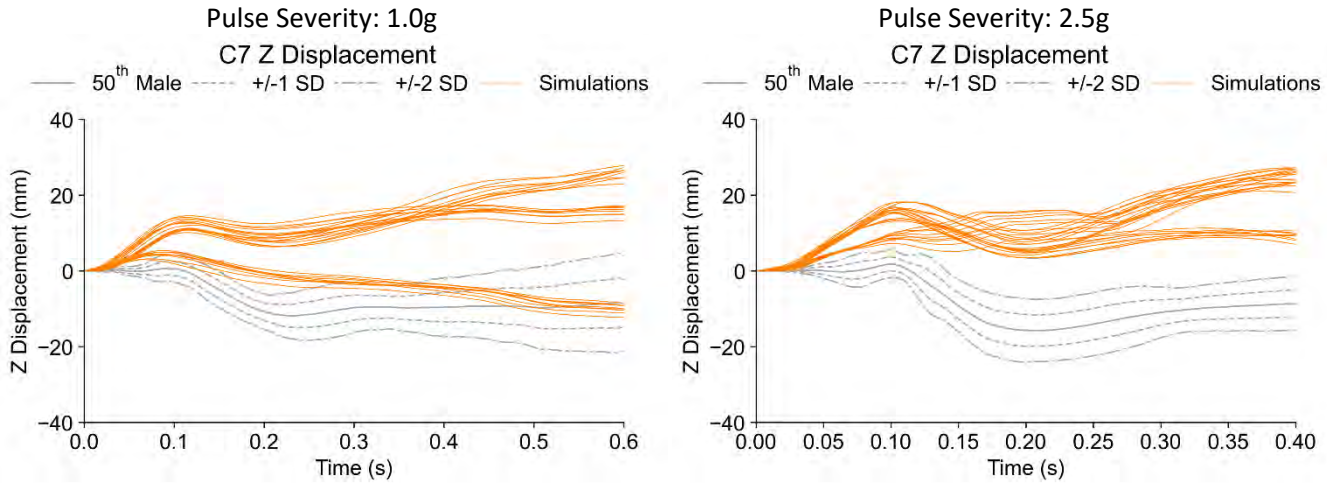

Fig. A 14. Comparison of C7 Z Displacement for all simulations with active muscles and experimental data (50th Male) for pre-crash braking (1g pulse severity: left) and low-speed impact event (2.5g pulse severity: right).

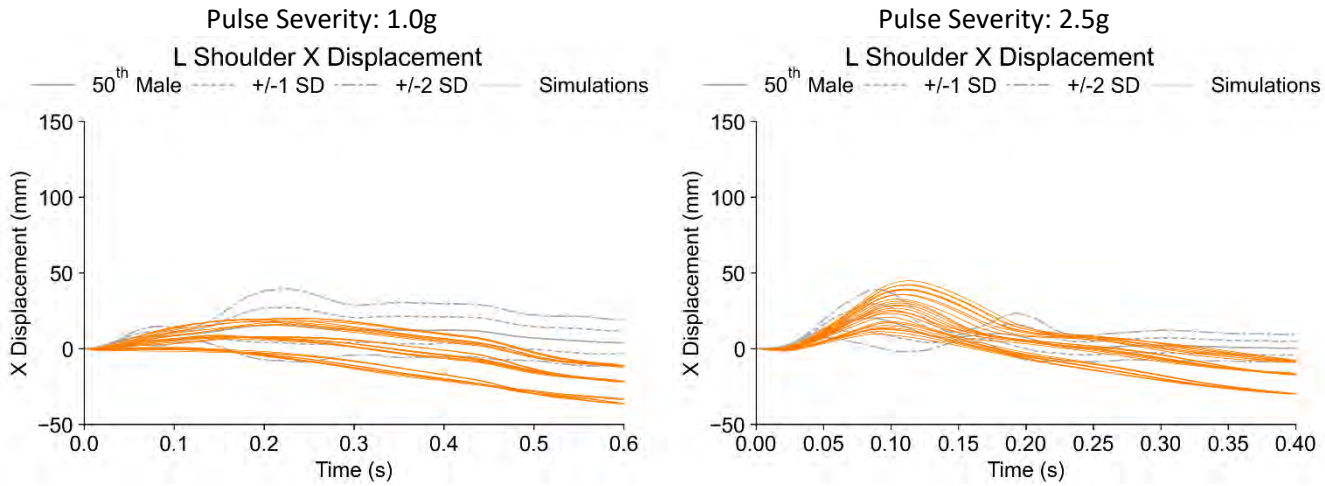

Fig. A 15. Comparison of L Shoulder X Displacement for all simulations with active muscles and experimental data (50th Male) for pre-crash braking (1g pulse severity: left) and low-speed impact event (2.5g pulse severity: right).

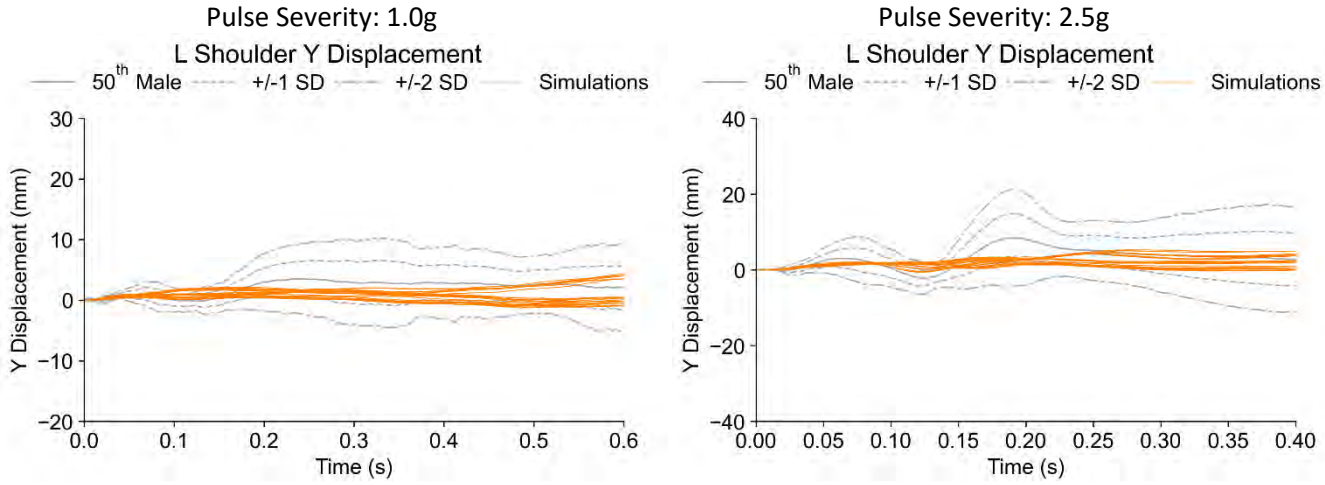

Fig. A 16. Comparison of L Shoulder Y Displacement for all simulations with active muscles and experimental data (50th Male) for pre-crash braking (1g pulse severity: left) and low-speed impact event (2.5g pulse severity: right).

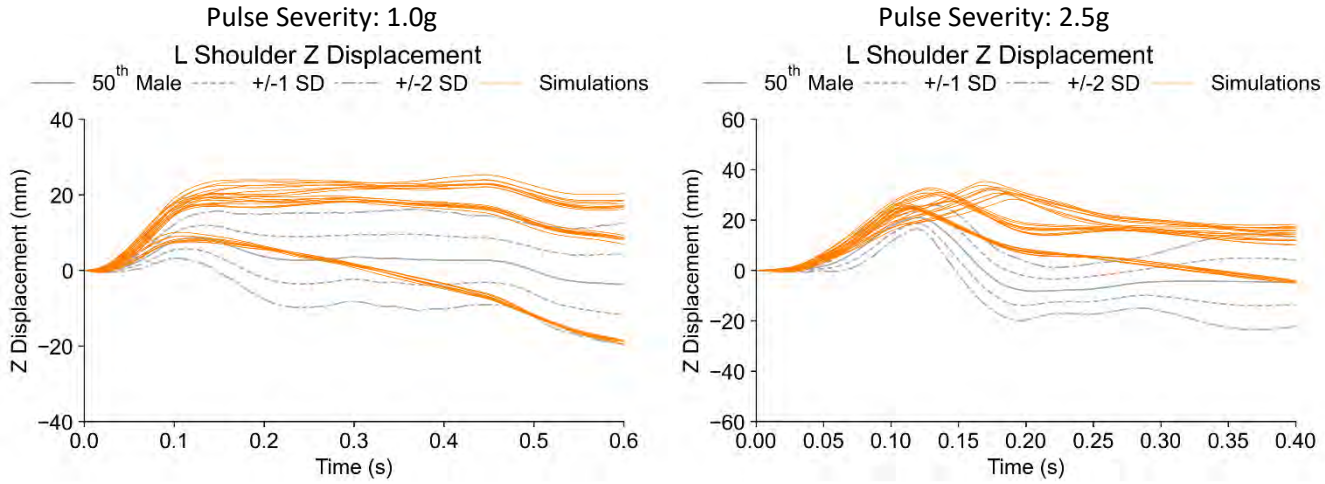

Fig. A 17. Comparison of L Shoulder Z Displacement for all simulations with active muscles and experimental data (50th Male) for pre-crash braking (1g pulse severity: left) and low-speed impact event (2.5g pulse severity: right).

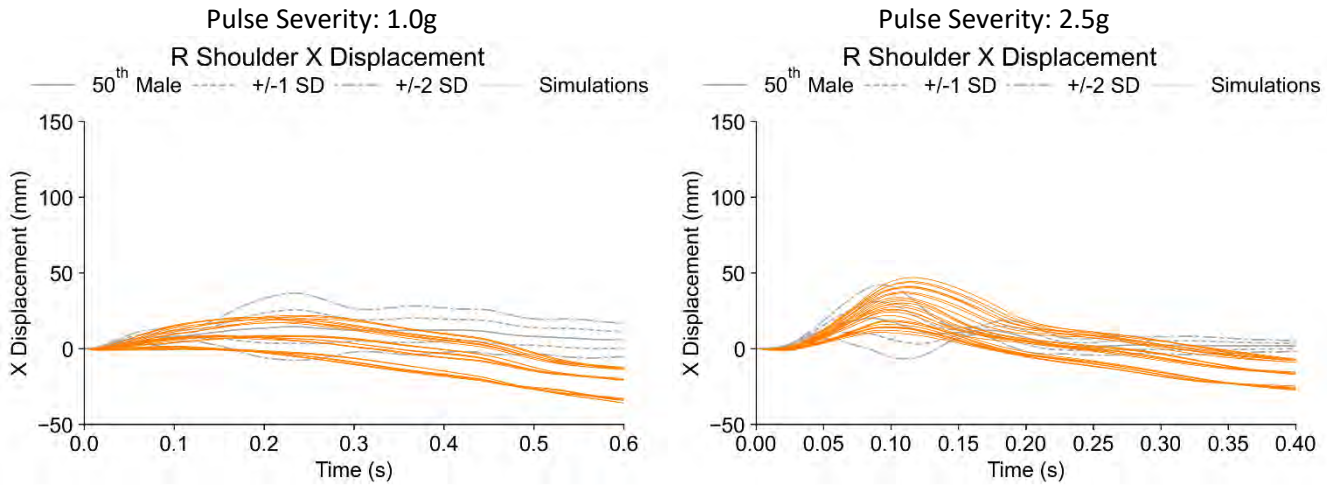

Fig. A 18. Comparison of R Shoulder X Displacement for all simulations with active muscles and experimental data (50th Male) for pre-crash braking (1g pulse severity: left) and low-speed impact event (2.5g pulse severity: right).

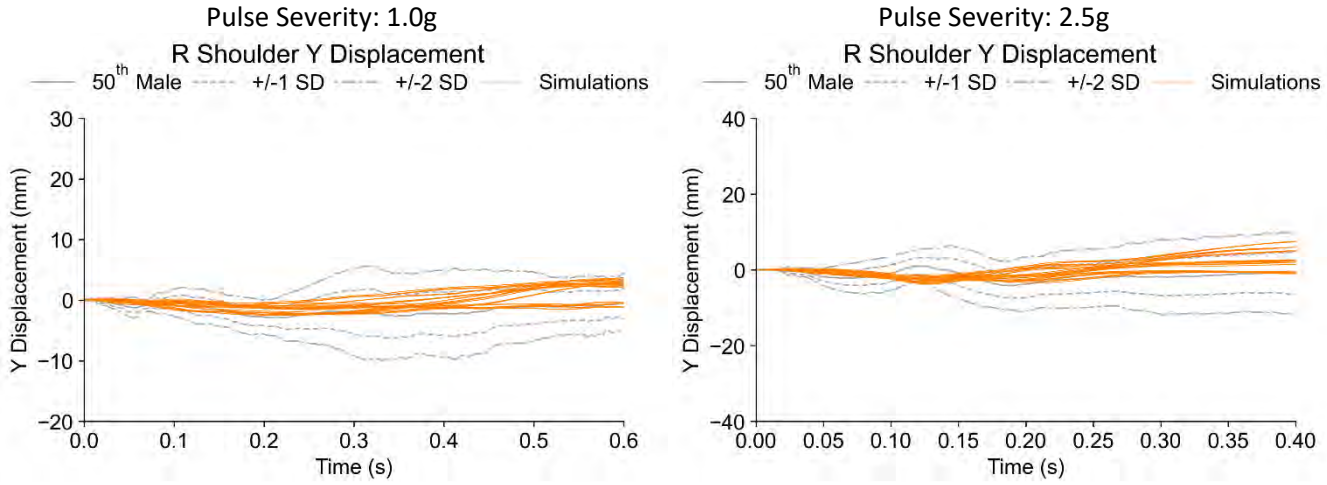

Fig. A 19. Comparison of R Shoulder Y Displacement for all simulations with active muscles and experimental data (50th Male) for pre-crash braking (1g pulse severity: left) and low-speed impact event (2.5g pulse severity: right).

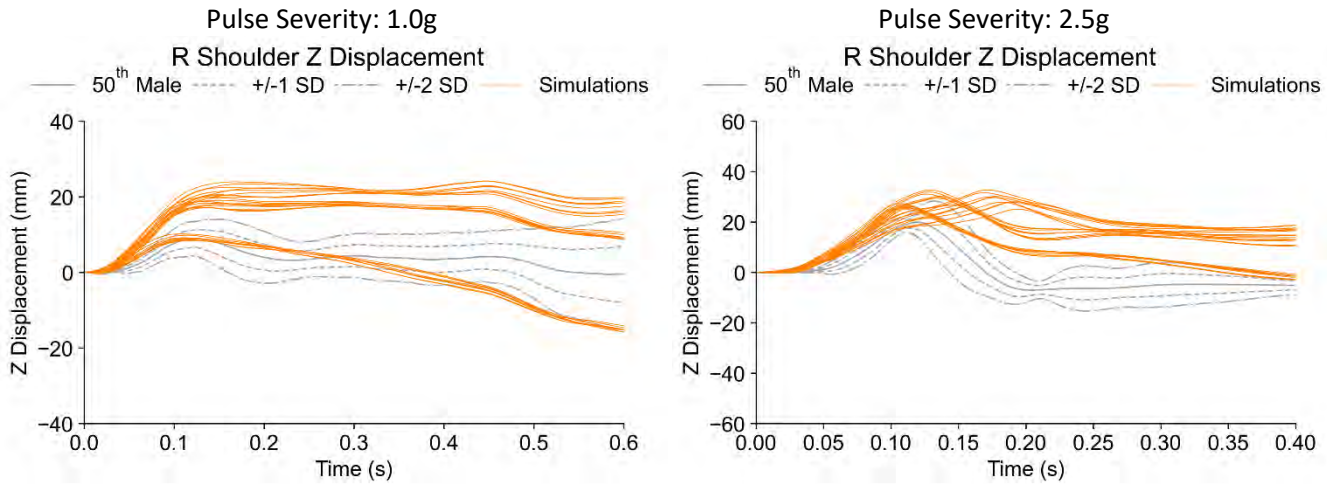

Fig. A 20. Comparison of R Shoulder Z Displacement for all simulations with active muscles and experimental data (50th Male) for pre-crash braking (1g pulse severity: left) and low-speed impact event (2.5g pulse severity: right).

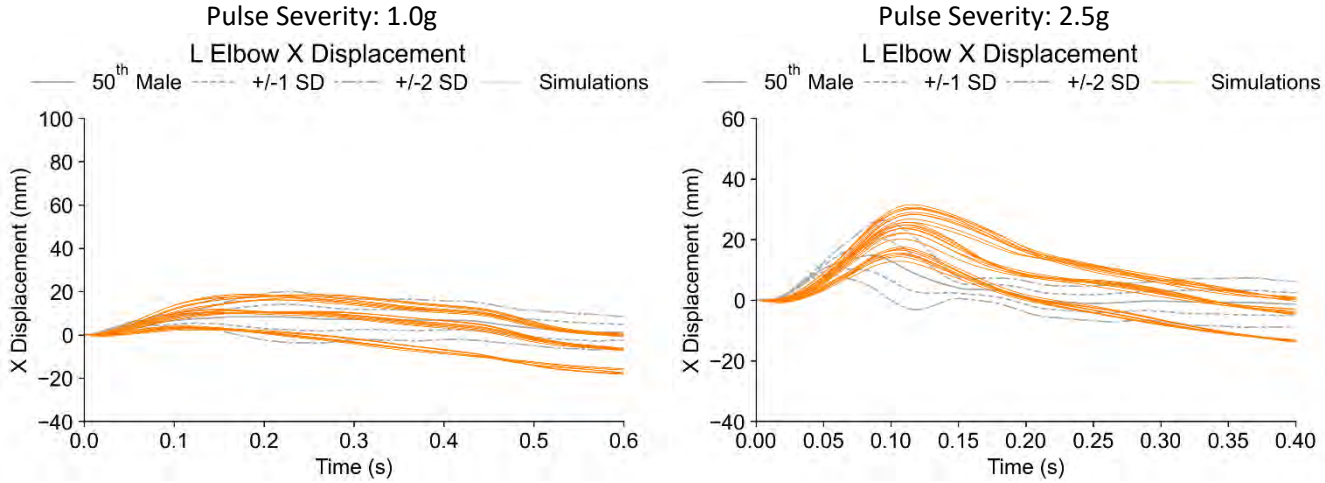

Fig. A 21. Comparison of L Elbow X Displacement for all simulations with active muscles and experimental data (50th Male) for pre-crash braking (1g pulse severity: left) and low-speed impact event (2.5g pulse severity: right).

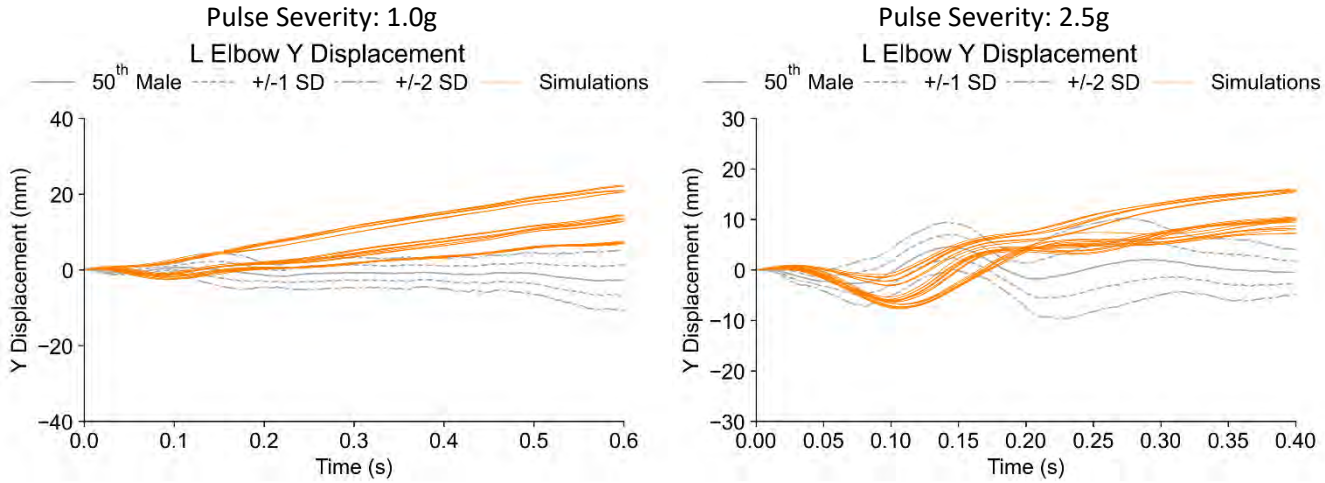

Fig. A 22. Comparison of L Elbow Y Displacement for all simulations with active muscles and experimental data (50th Male) for pre-crash braking (1g pulse severity: left) and low-speed impact event (2.5g pulse severity: right).

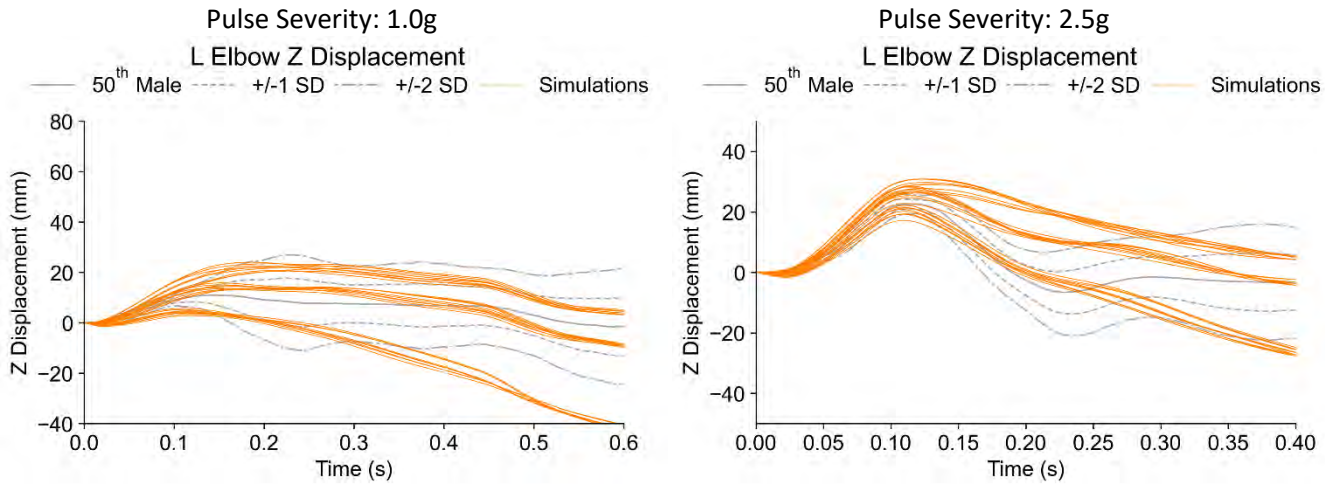

Fig. A 23. Comparison of L Elbow Z Displacement for all simulations with active muscles and experimental data (50th Male) for pre-crash braking (1g pulse severity: left) and low-speed impact event (2.5g pulse severity: right).

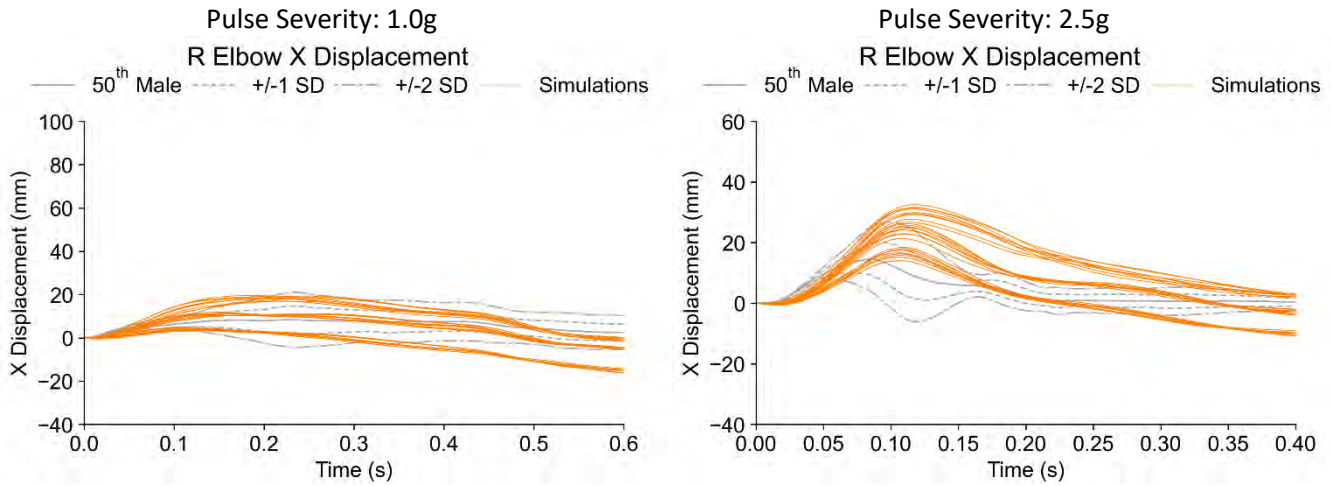

Fig. A 24. Comparison of R Elbow X Displacement for all simulations with active muscles and experimental data (50th Male) for pre-crash braking (1g pulse severity: left) and low-speed impact event (2.5g pulse severity: right).

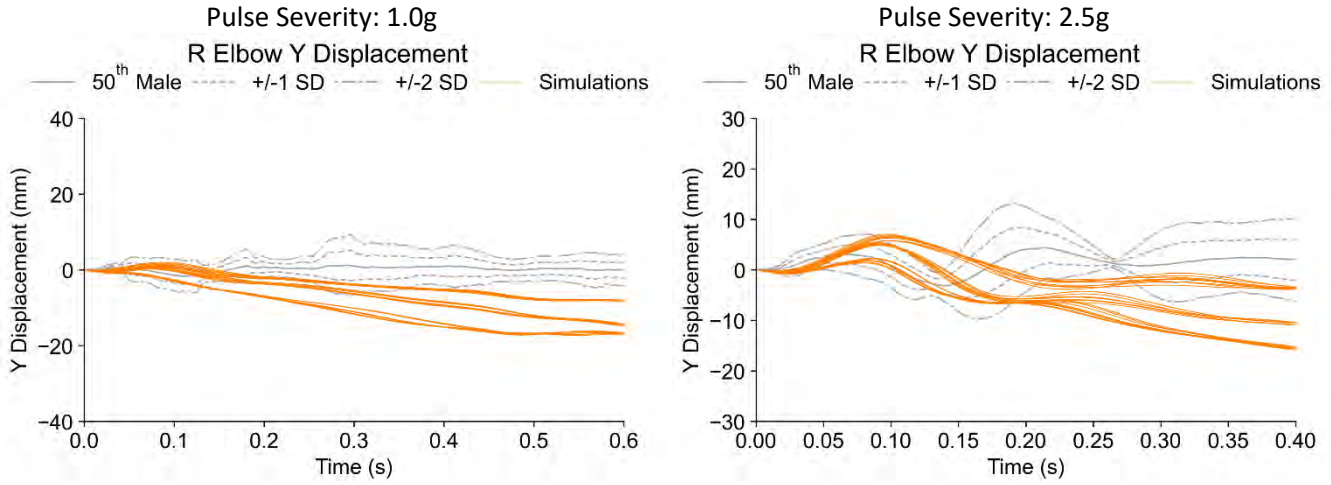

Fig. A 25. Comparison of R Elbow Y Displacement for all simulations with active muscles and experimental data (50th Male) for pre-crash braking (1g pulse severity: left) and low-speed impact event (2.5g pulse severity: right).

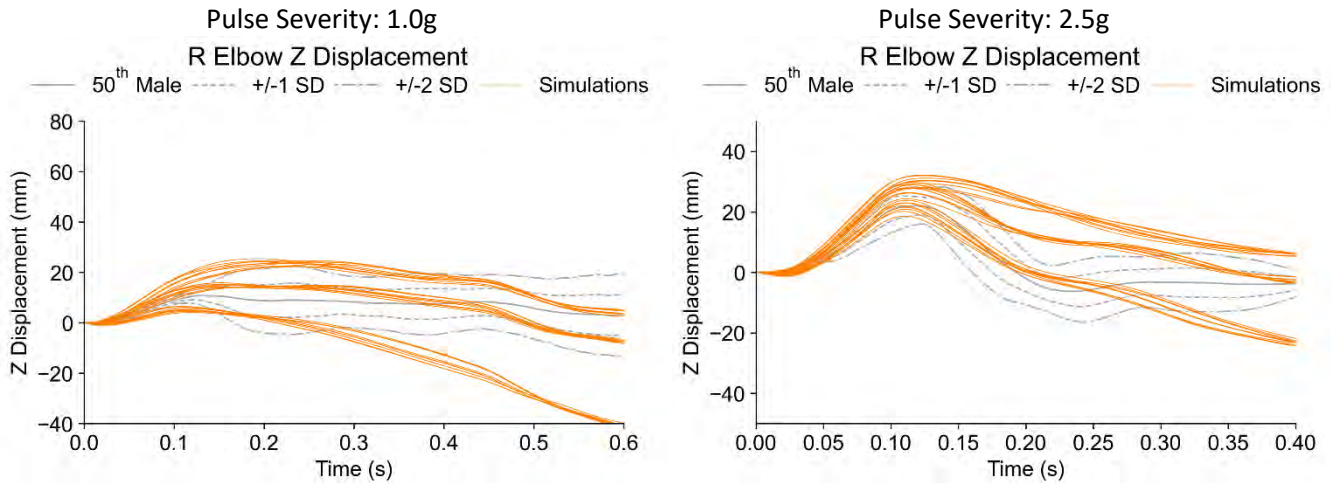

Fig. A 26. Comparison of R Elbow Z Displacement for all simulations with active muscles and experimental data (50th Male) for pre-crash braking (1g pulse severity: left) and low-speed impact event (2.5g pulse severity: right).

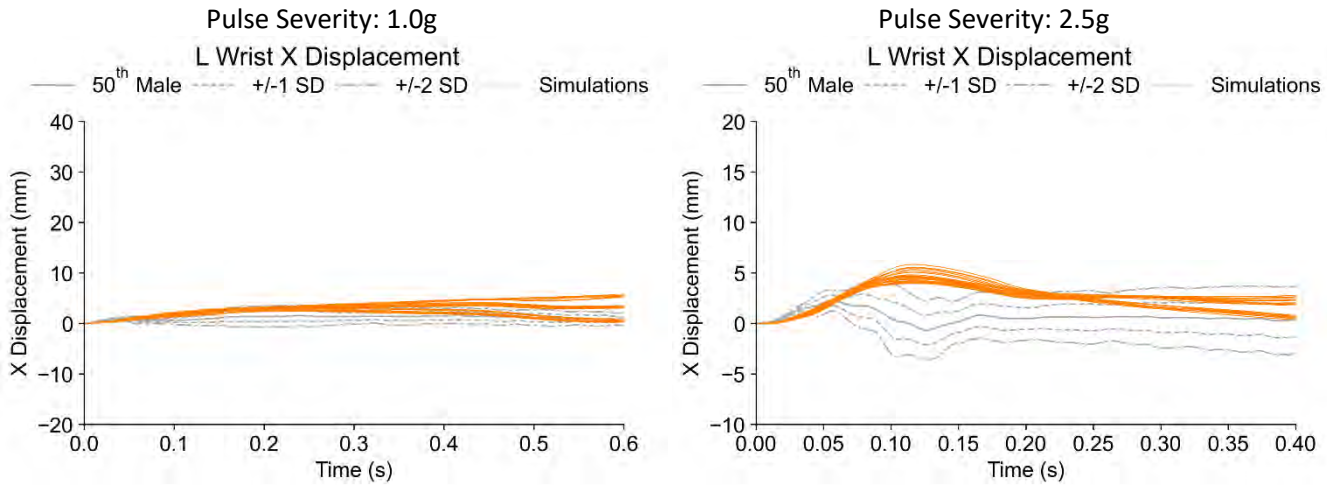

Fig. A 27. Comparison of L Wrist X Displacement for all simulations with active muscles and experimental data (50th Male) for pre-crash braking (1g pulse severity: left) and low-speed impact event (2.5g pulse severity: right).

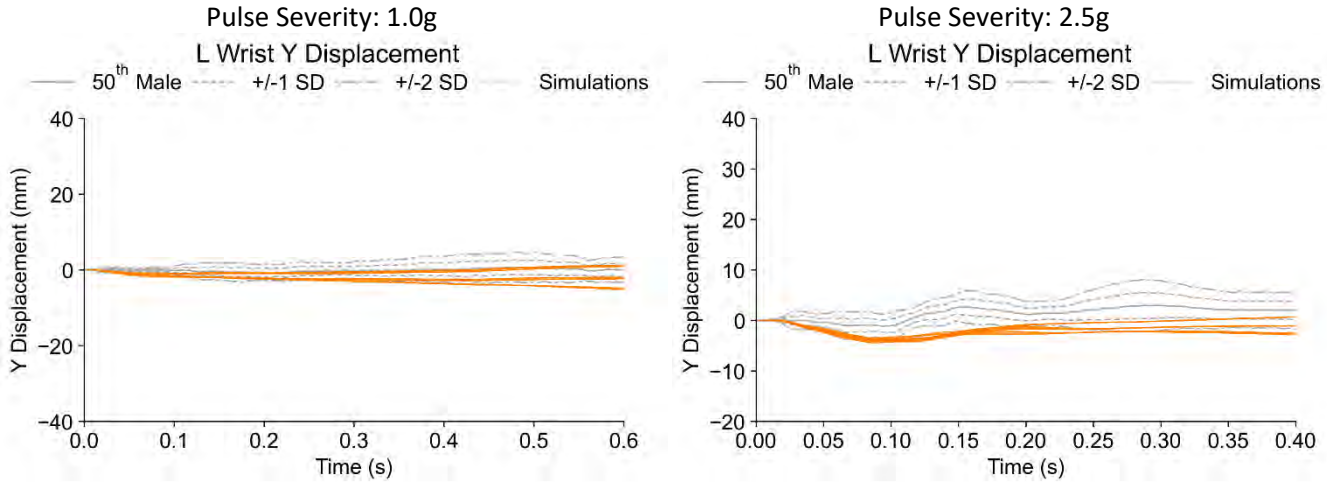

Fig. A 28. Comparison of L Wrist Y Displacement for all simulations with active muscles and experimental data (50th Male) for pre-crash braking (1g pulse severity: left) and low-speed impact event (2.5g pulse severity: right).

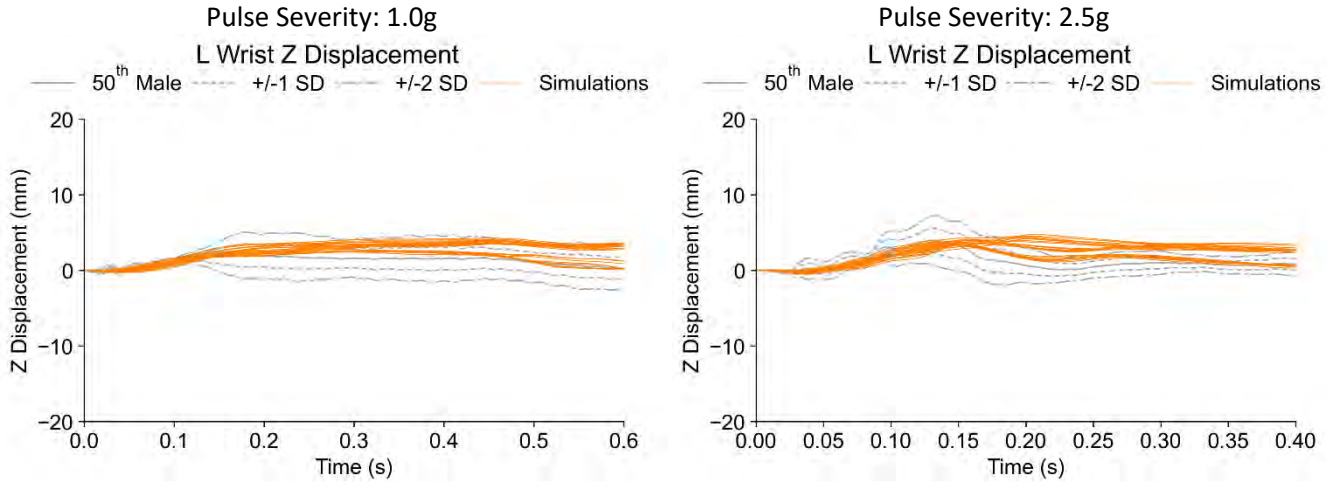

Fig. A 29. Comparison of L Wrist Z Displacement for all simulations with active muscles and experimental data (50th Male) for pre-crash braking (1g pulse severity: left) and low-speed impact event (2.5g pulse severity: right).

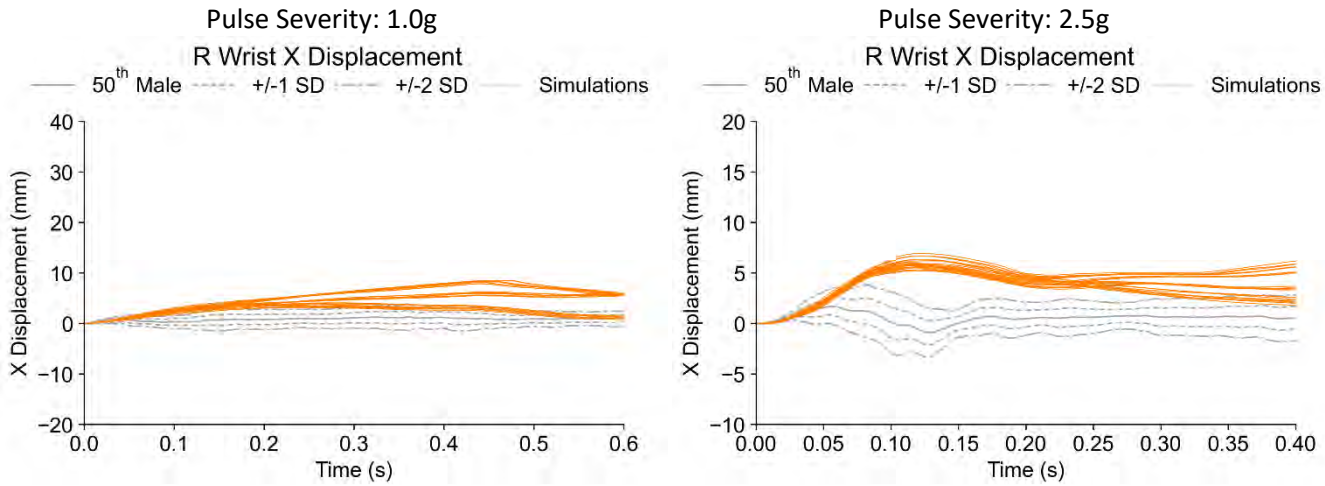

Fig. A 30. Comparison of R Wrist X Displacement for all simulations with active muscles and experimental data (50th Male) for pre-crash braking (1g pulse severity: left) and low-speed impact event (2.5g pulse severity: right).

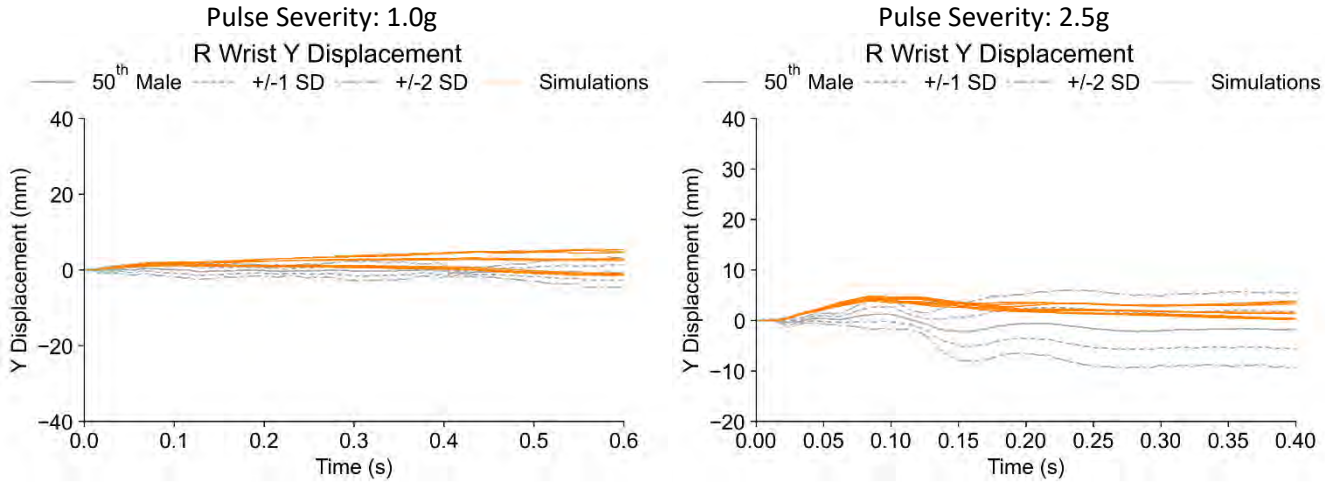

Fig. A 31. Comparison of R Wrist Y Displacement for all simulations with active muscles and experimental data (50th Male) for pre-crash braking (1g pulse severity: left) and low-speed impact event (2.5g pulse severity: right).

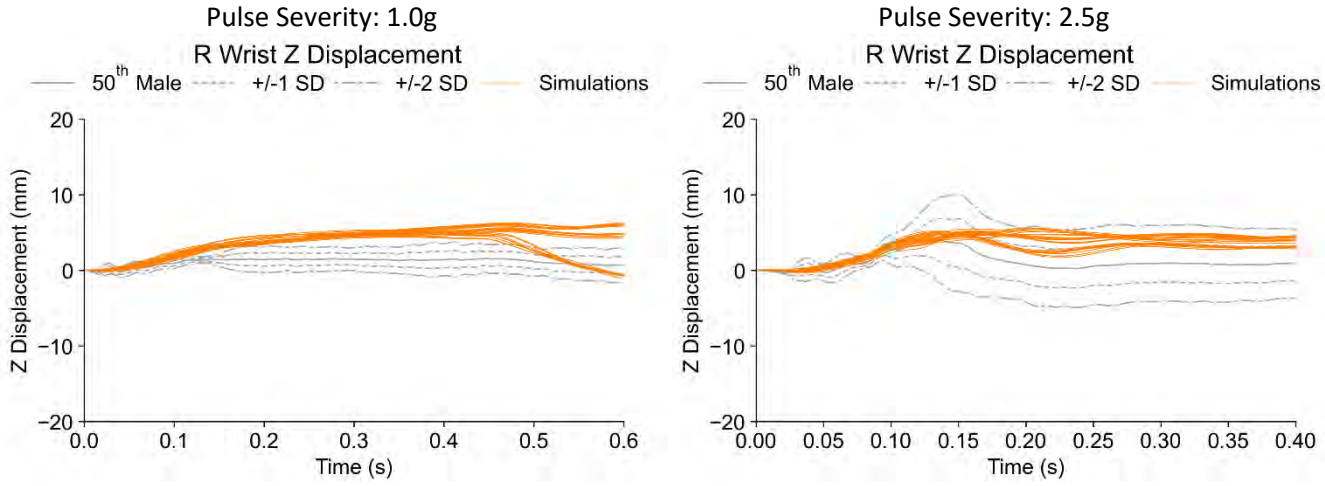

Fig. A 32. Comparison of R Wrist Z Displacement for all simulations with active muscles and experimental data (50th Male) for pre-crash braking (1g pulse severity: left) and low-speed impact event (2.5g pulse severity: right).

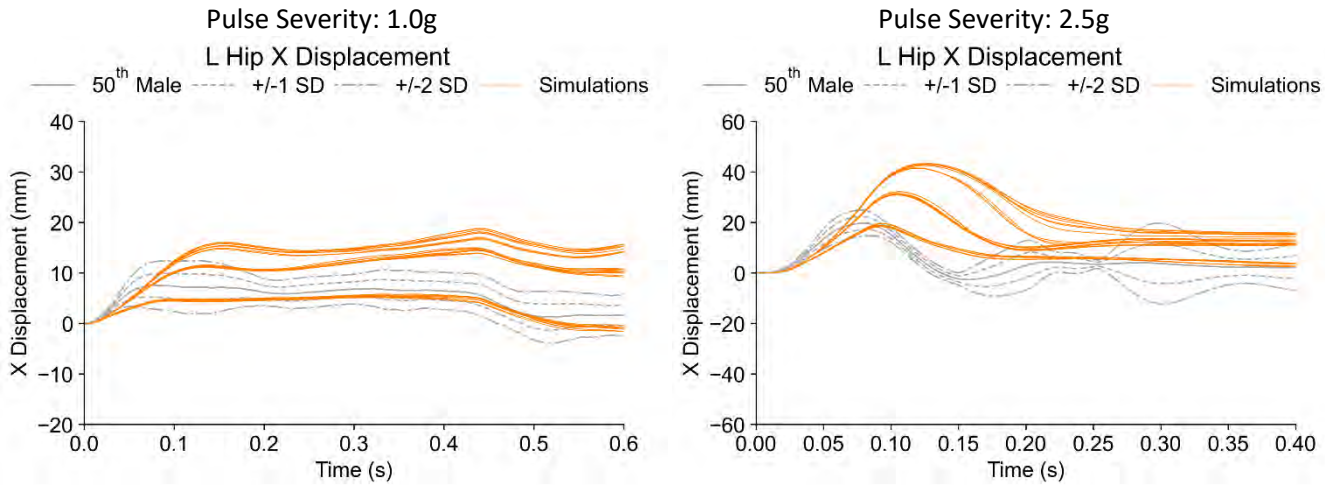

Fig. A 33. Comparison of L Hip X Displacement for all simulations with active muscles and experimental data (50th Male) for pre-crash braking (1g pulse severity: left) and low-speed impact event (2.5g pulse severity: right).

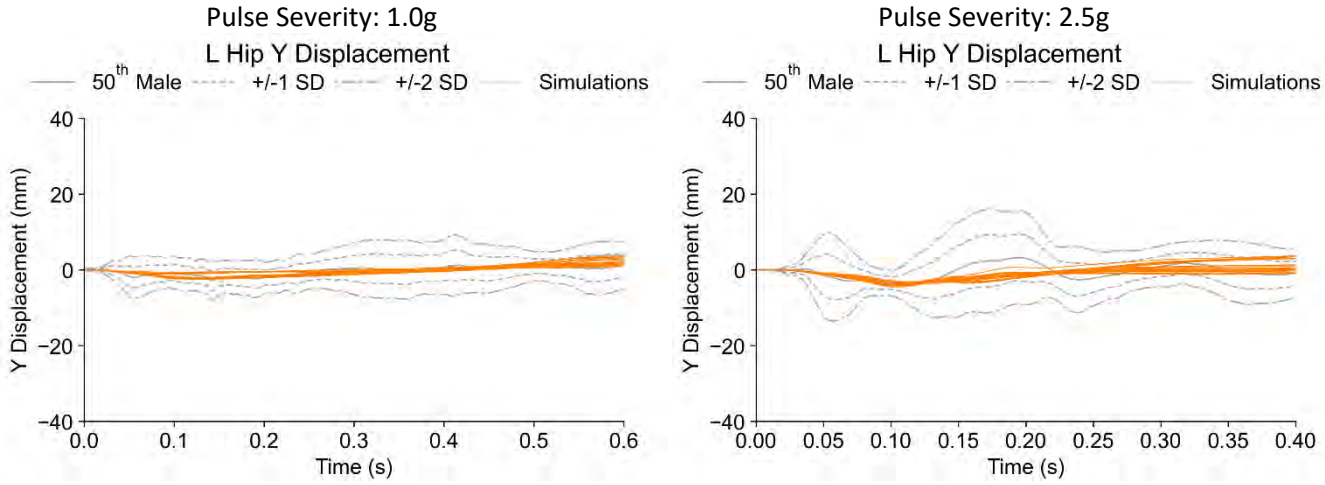

Fig. A 34. Comparison of L Hip Y Displacement for all simulations with active muscles and experimental data (50th Male) for pre-crash braking (1g pulse severity: left) and low-speed impact event (2.5g pulse severity: right).

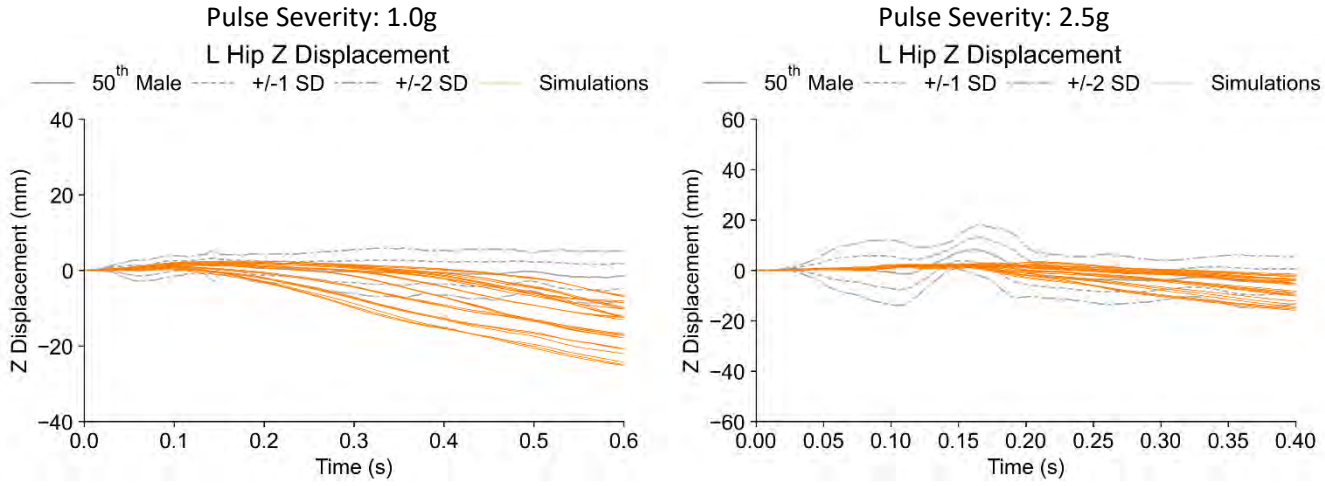

Fig. A 35. Comparison of L Hip Z Displacement for all simulations with active muscles and experimental data (50th Male) for pre-crash braking (1g pulse severity: left) and low-speed impact event (2.5g pulse severity: right).

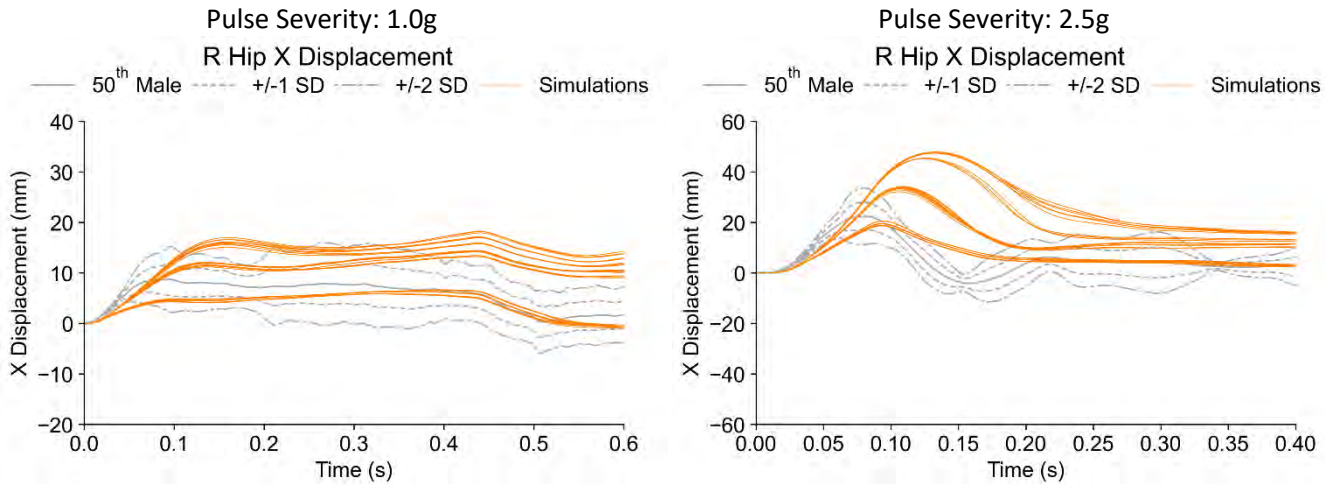

Fig. A 36. Comparison of R Hip X Displacement for all simulations with active muscles and experimental data (50th Male) for pre-crash braking (1g pulse severity: left) and low-speed impact event (2.5g pulse severity: right).

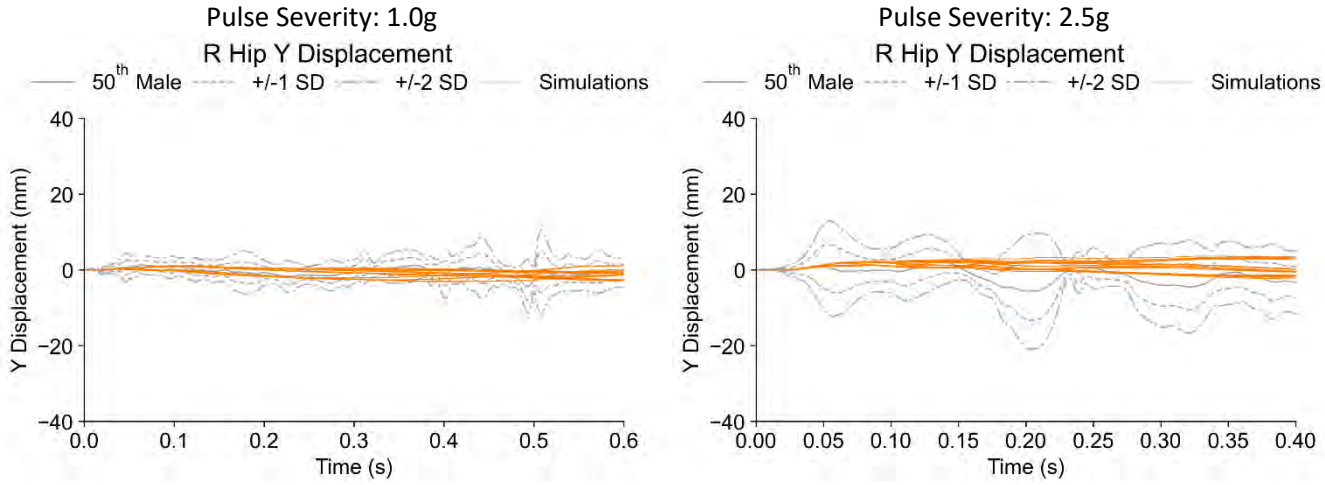

Fig. A 37. Comparison of R Hip Y Displacement for all simulations with active muscles and experimental data (50th Male) for pre-crash braking (1g pulse severity: left) and low-speed impact event (2.5g pulse severity: right).

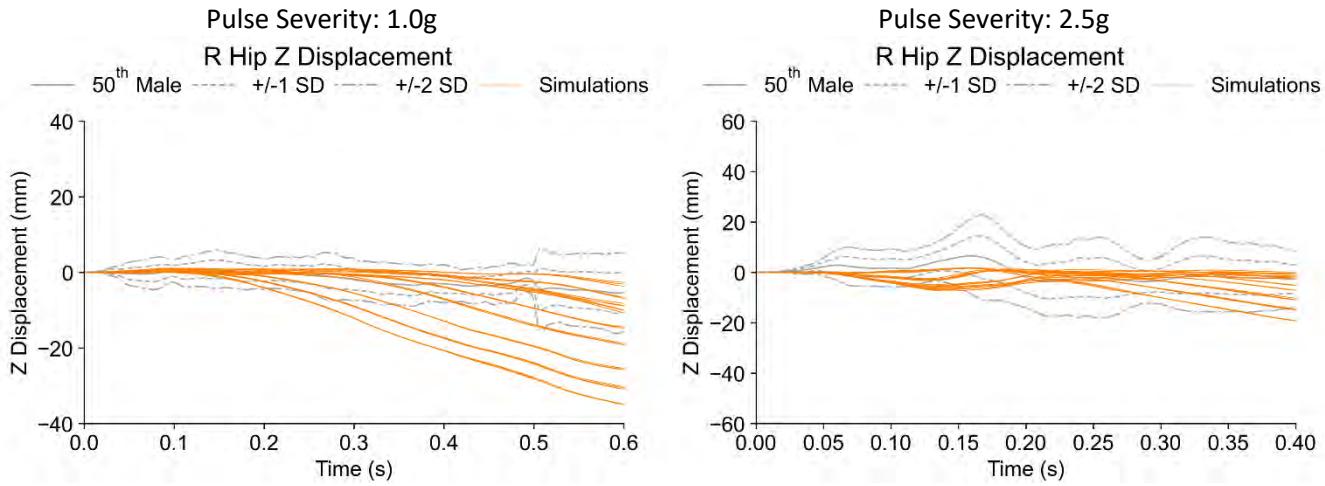

Fig. A 38. Comparison of R Hip Z Displacement for all simulations with active muscles and experimental data (50th Male) for pre-crash braking (1g pulse severity: left) and low-speed impact event (2.5g pulse severity: right).

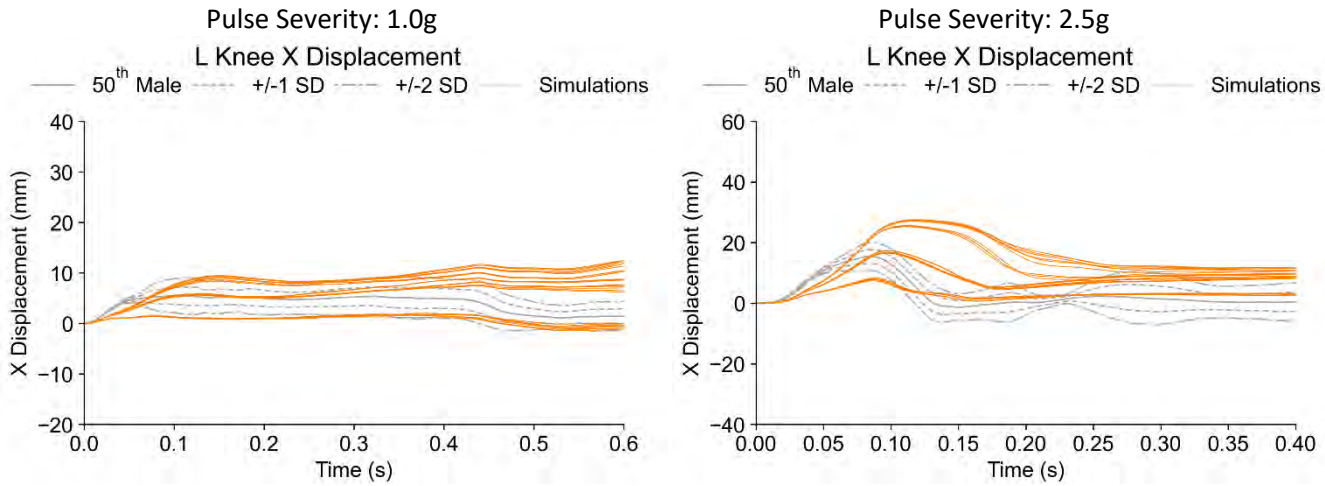

Fig. A 39. Comparison of L Knee X Displacement for all simulations with active muscles and experimental data (50th Male) for pre-crash braking (1g pulse severity: left) and low-speed impact event (2.5g pulse severity: right).

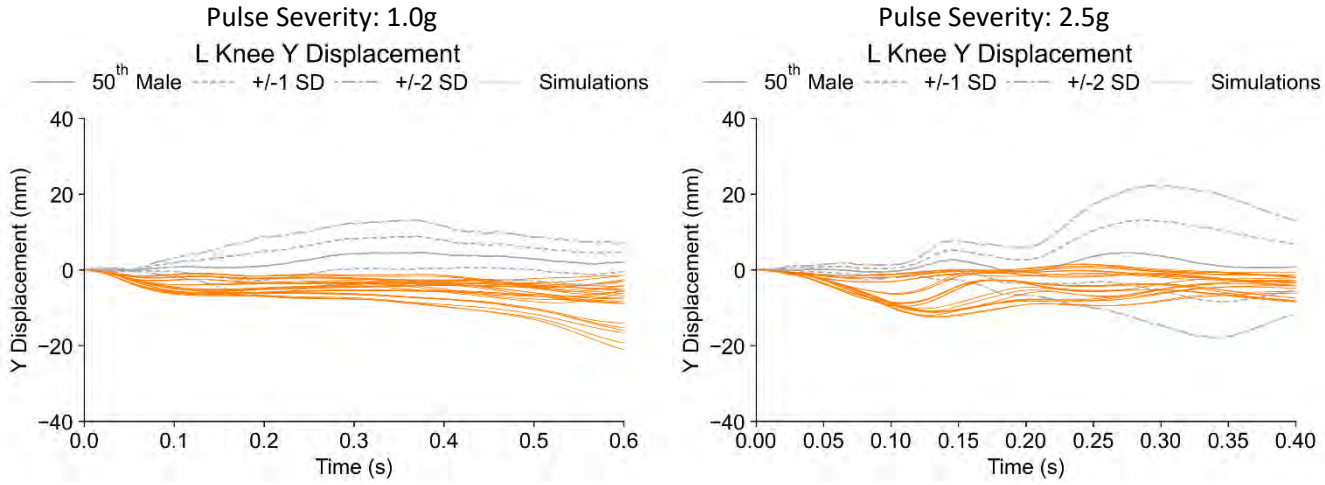

Fig. A 40. Comparison of L Knee Y Displacement for all simulations with active muscles and experimental data (50th Male) for pre-crash braking (1g pulse severity: left) and low-speed impact event (2.5g pulse severity: right).

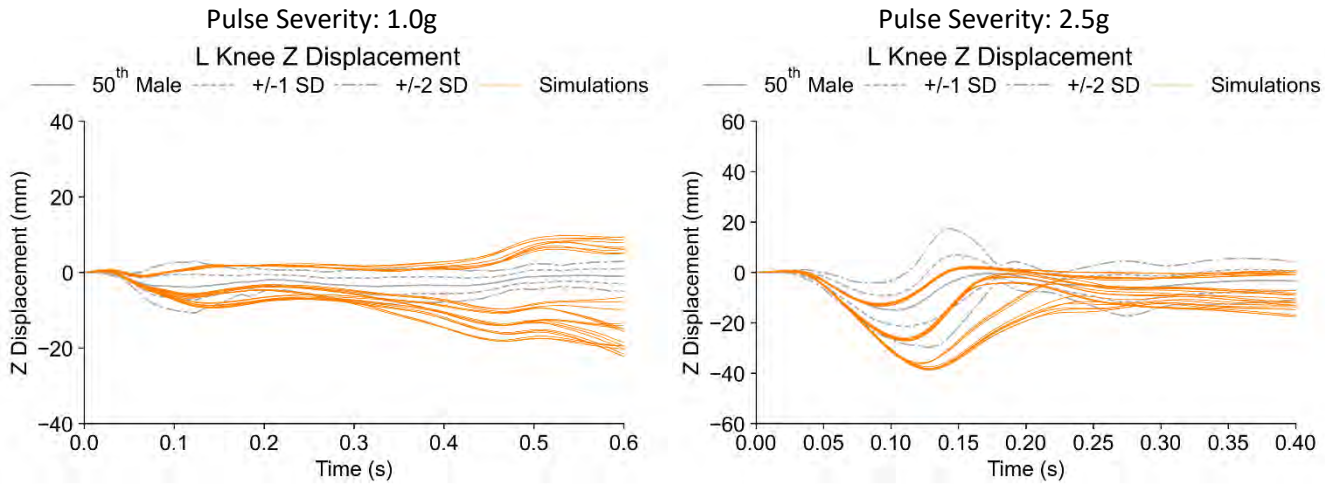

Fig. A 41. Comparison of L Knee Z Displacement for all simulations with active muscles and experimental data (50th Male) for pre-crash braking (1g pulse severity: left) and low-speed impact event (2.5g pulse severity: right).

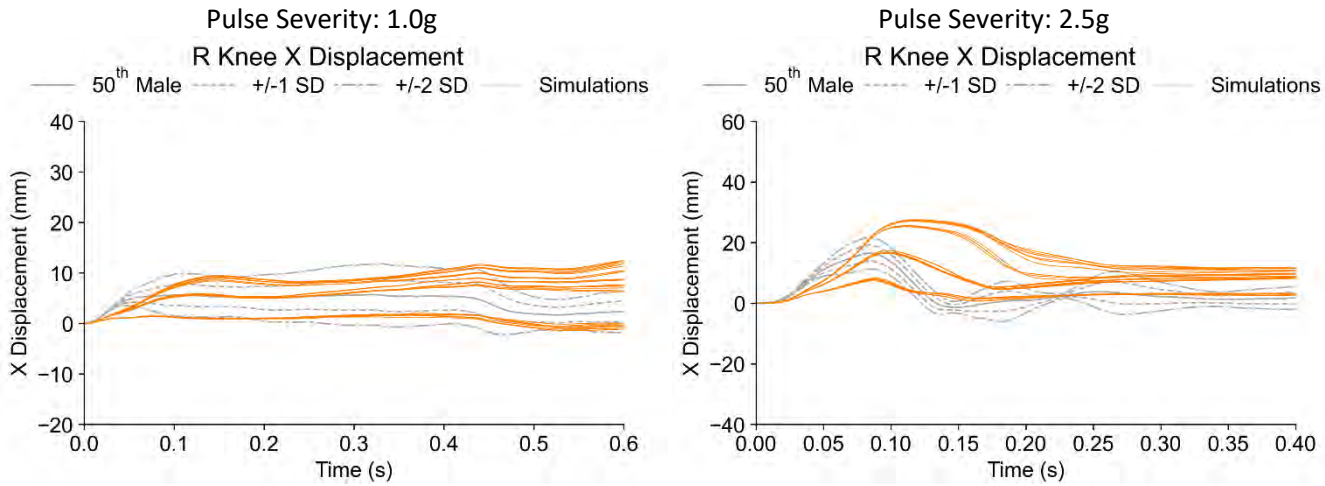

Fig. A 42. Comparison of R Knee X Displacement for all simulations with active muscles and experimental data (50th Male) for pre-crash braking (1g pulse severity: left) and low-speed impact event (2.5g pulse severity: right).

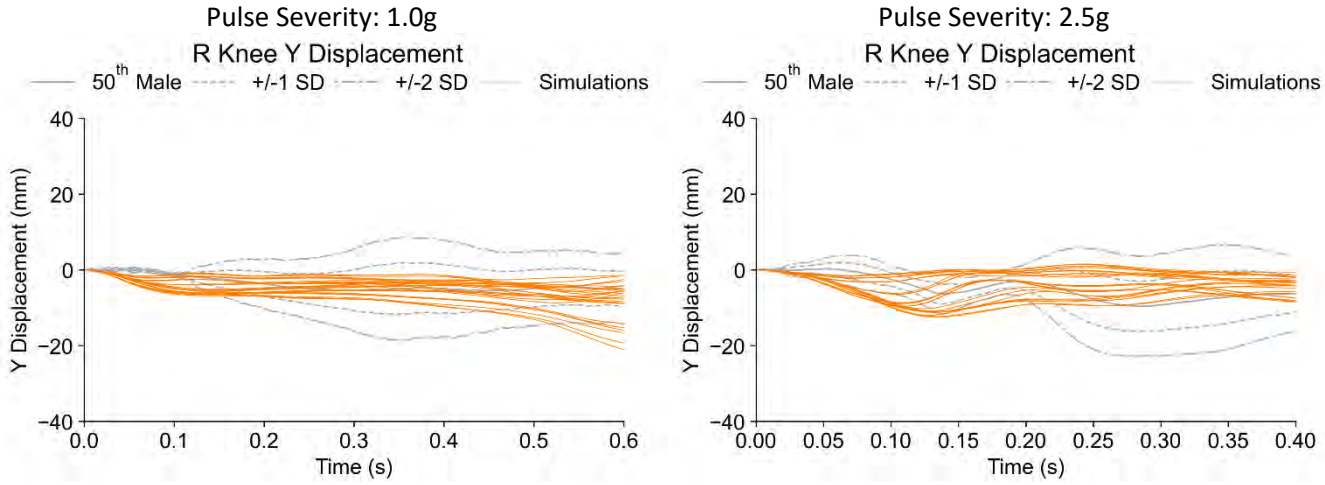

Fig. A 43. Comparison of R Knee Y Displacement for all simulations with active muscles and experimental data (50th Male) for pre-crash braking (1g pulse severity: left) and low-speed impact event (2.5g pulse severity: right).

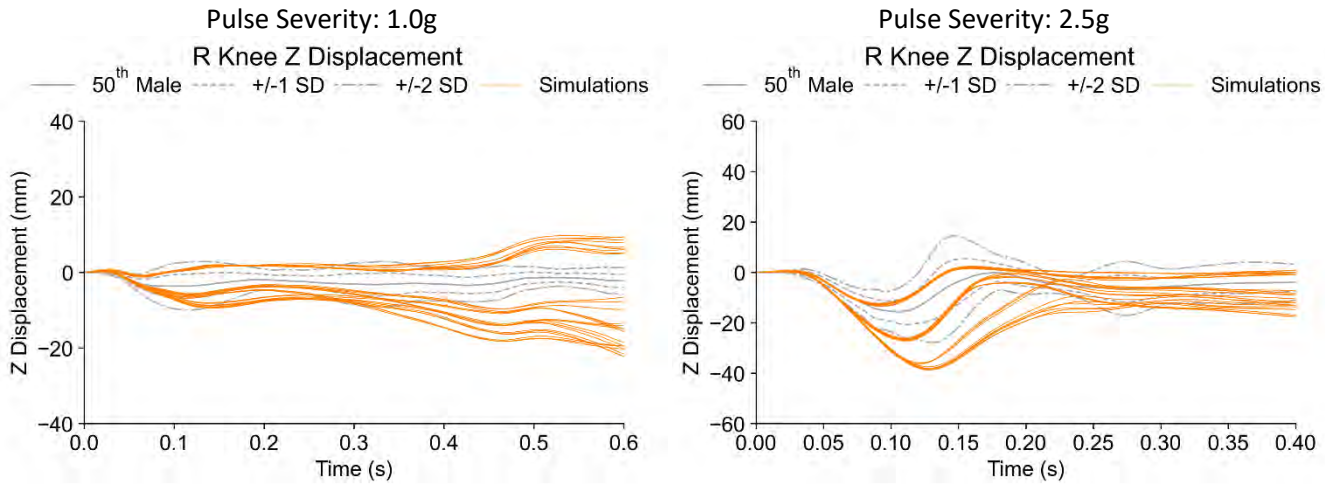

Fig. A 44. Comparison of R Knee Z Displacement for all simulations with active muscles and experimental data (50th Male) for pre-crash braking (1g pulse severity: left) and low-speed impact event (2.5g pulse severity: right).

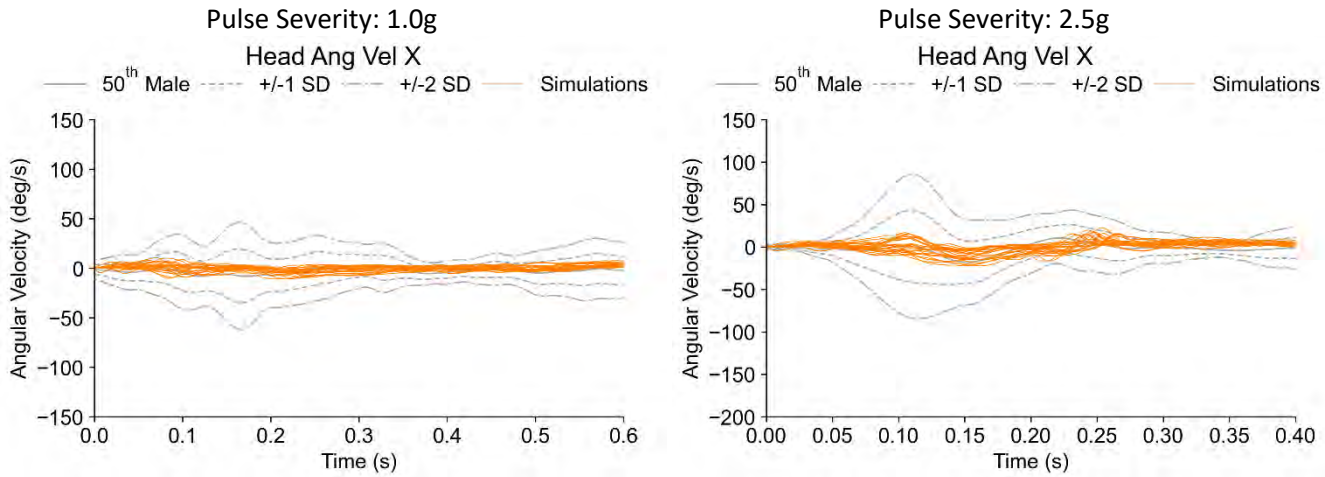

Fig. A 45. Comparison of Head Ang Vel X for all simulations with active muscles and experimental data (50th Male) for pre-crash braking (1g pulse severity: left) and low-speed impact event (2.5g pulse severity: right).

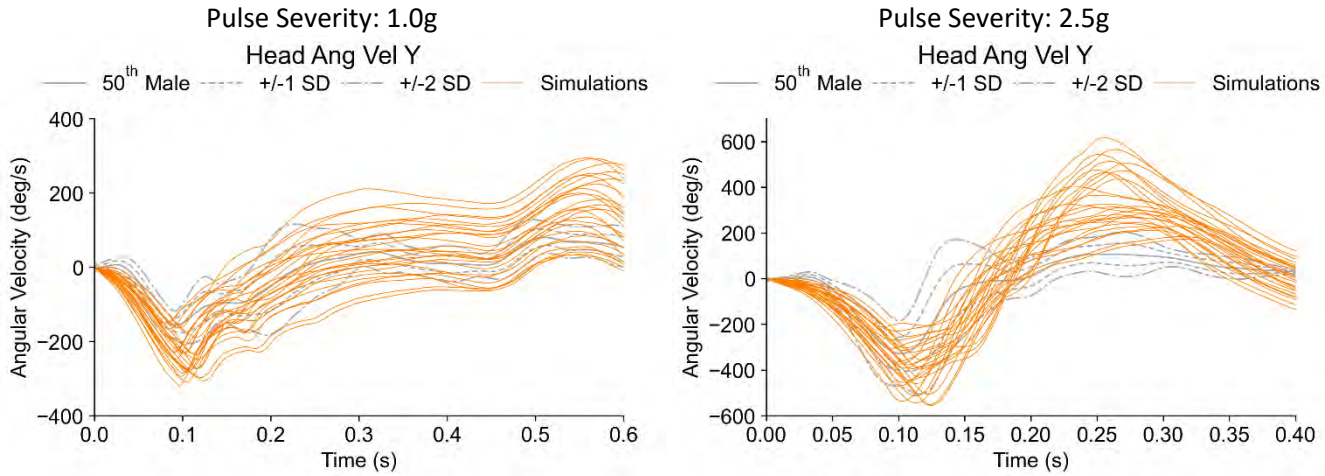

Fig. A 46. Comparison of Head Ang Vel Y for all simulations with active muscles and experimental data (50th Male) for pre-crash braking (1g pulse severity: left) and low-speed impact event (2.5g pulse severity: right).

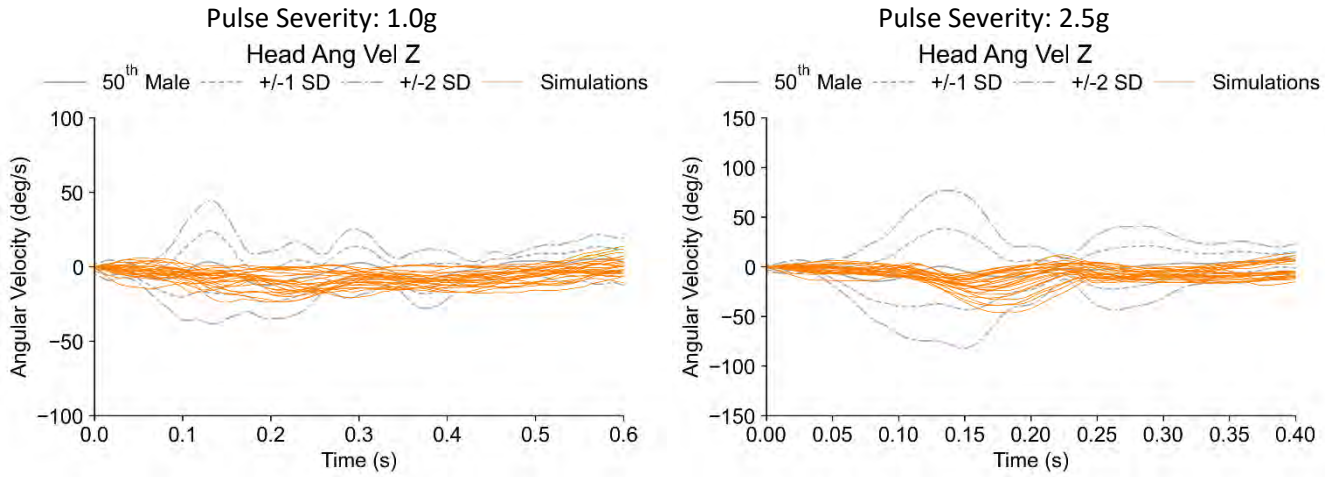

Fig. A 47. Comparison of Head Ang Vel Z for all simulations with active muscles and experimental data (50th Male) for pre-crash braking (1g pulse severity: left) and low-speed impact event (2.5g pulse severity: right).

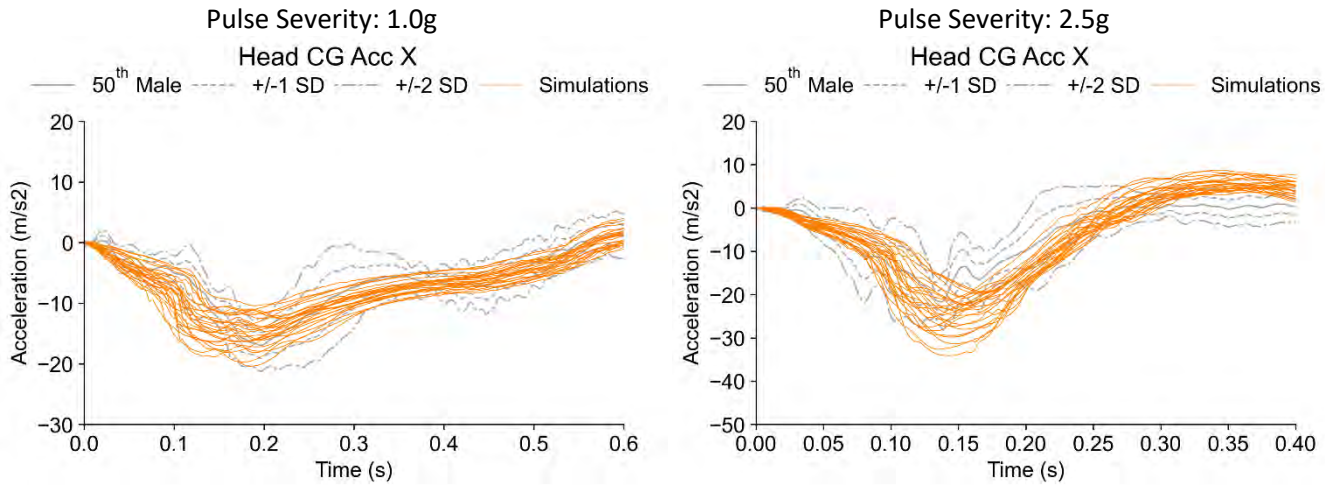

Fig. A 48. Comparison of Head CG Acc X for all simulations with active muscles and experimental data (50th Male) for pre-crash braking (1g pulse severity: left) and low-speed impact event (2.5g pulse severity: right).

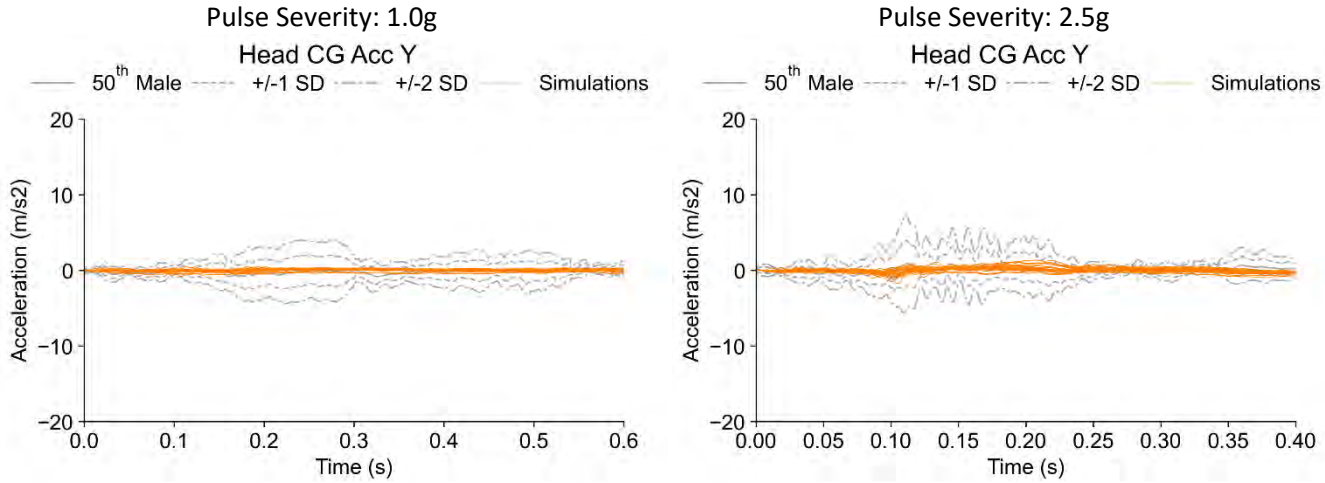

Fig. A 49. Comparison of Head CG Acc Y for all simulations with active muscles and experimental data (50th Male) for pre-crash braking (1g pulse severity: left) and low-speed impact event (2.5g pulse severity: right).

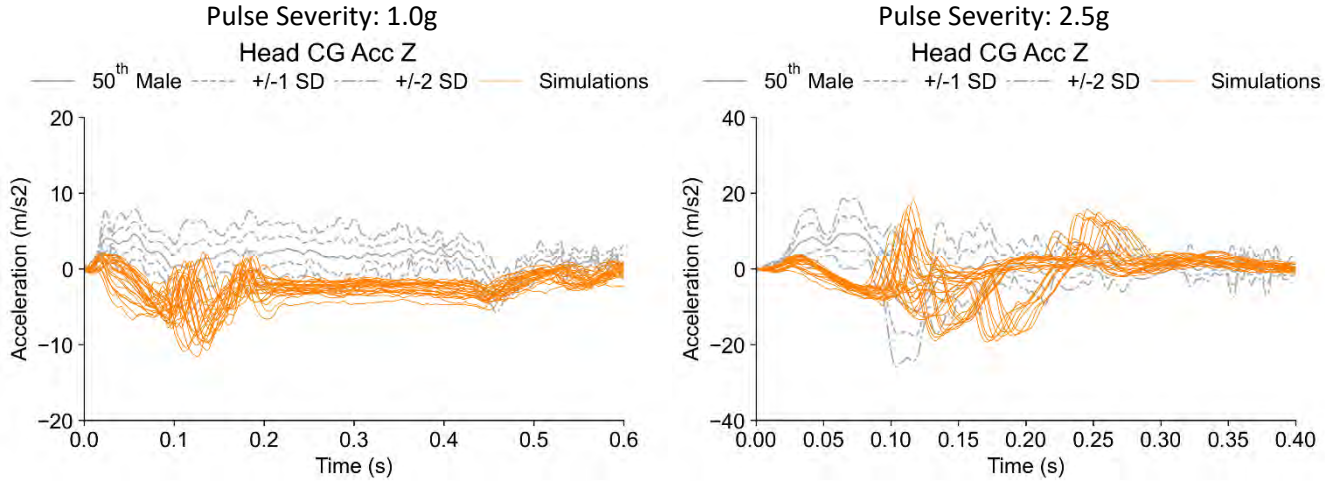

Fig. A 50. Comparison of Head CG Acc Z for all simulations with active muscles and experimental data (50th Male) for pre-crash braking (1g pulse severity: left) and low-speed impact event (2.5g pulse severity: right).

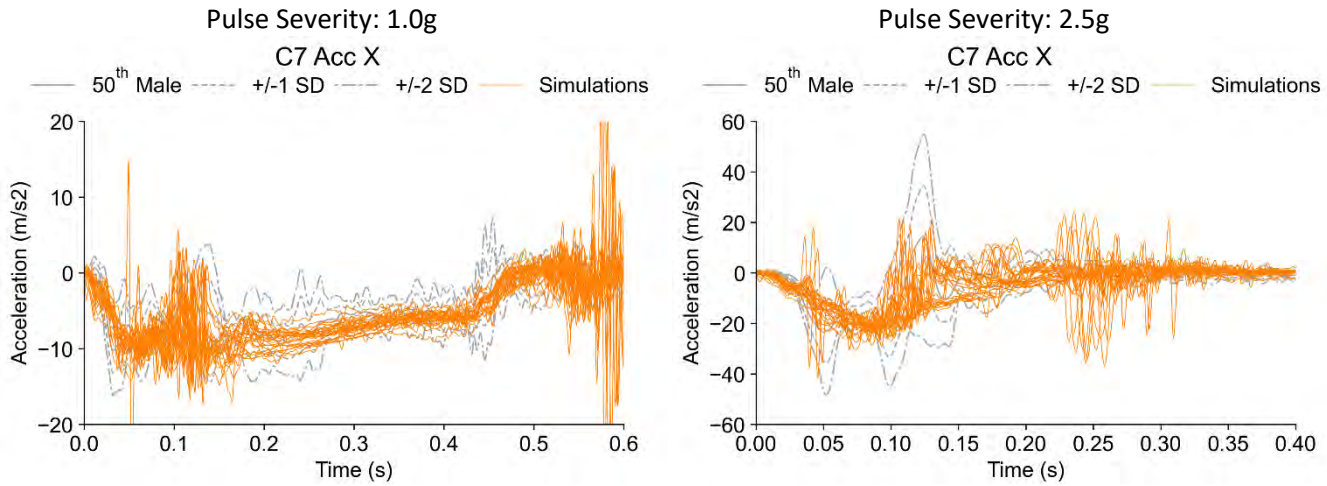

Fig. A 51. Comparison of C7 Acc X for all simulations with active muscles and experimental data (50th Male) for pre-crash braking (1g pulse severity: left) and low-speed impact event (2.5g pulse severity: right).

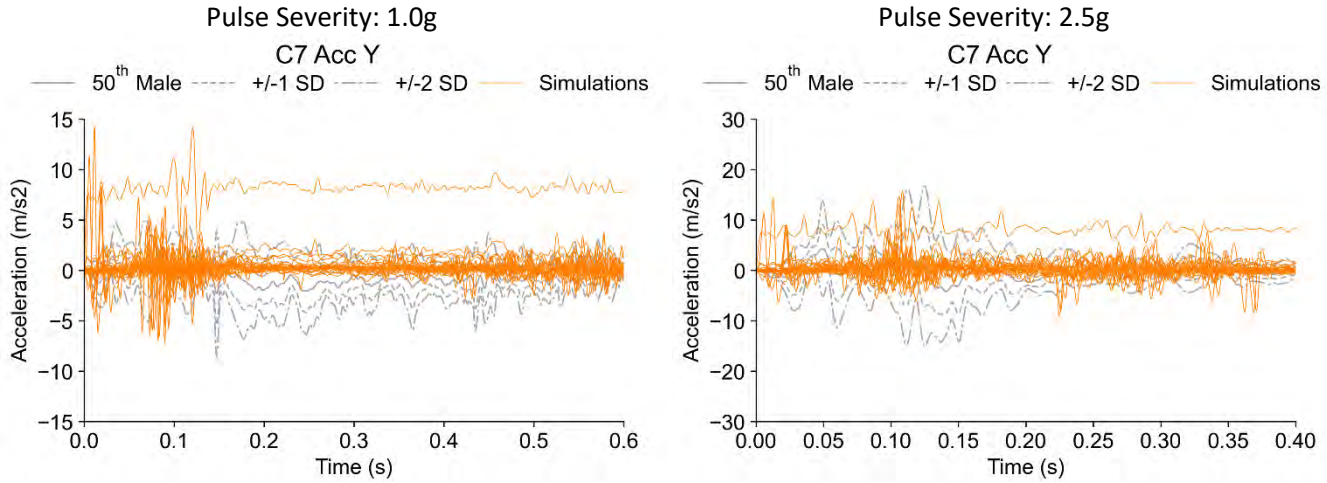

Fig. A 52. Comparison of C7 Acc Y for all simulations with active muscles and experimental data (50th Male) for pre-crash braking (1g pulse severity: left) and low-speed impact event (2.5g pulse severity: right).

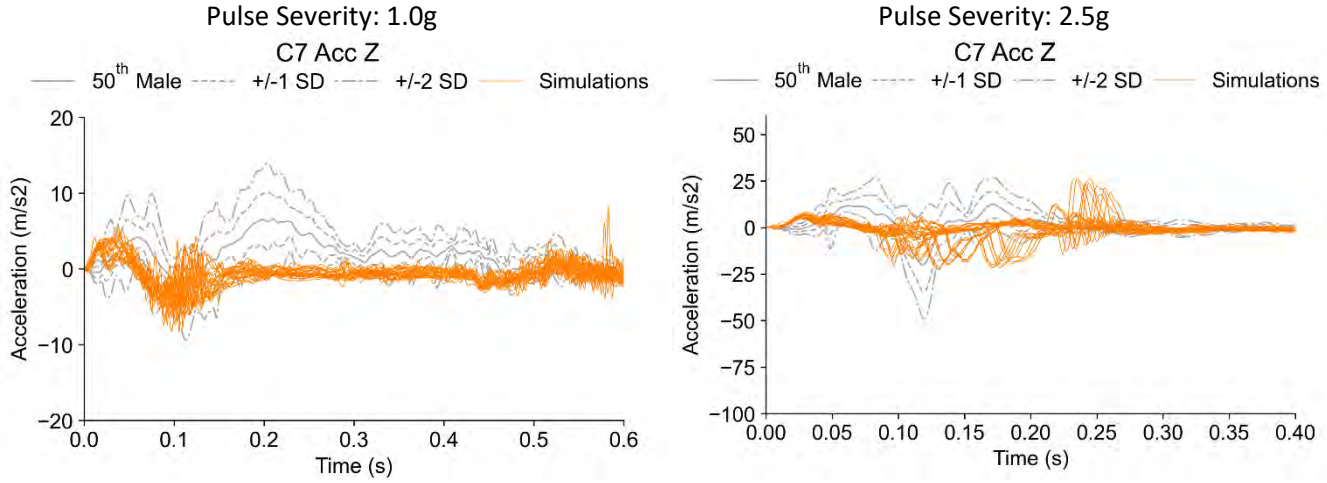

Fig. A 53. Comparison of C7 Acc Z for all simulations with active muscles and experimental data (50th Male) for pre-crash braking (1g pulse severity: left) and low-speed impact event (2.5g pulse severity: right).

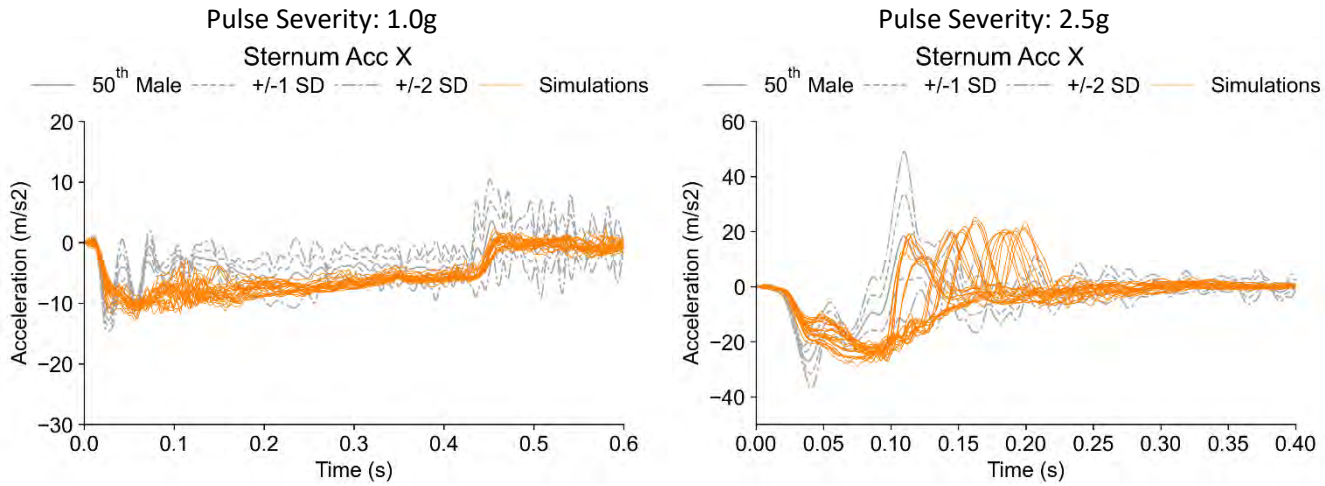

Fig. A 54. Comparison of Sternum Acc X for all simulations with active muscles and experimental data (50th Male) for pre-crash braking (1g pulse severity: left) and low-speed impact event (2.5g pulse severity: right).

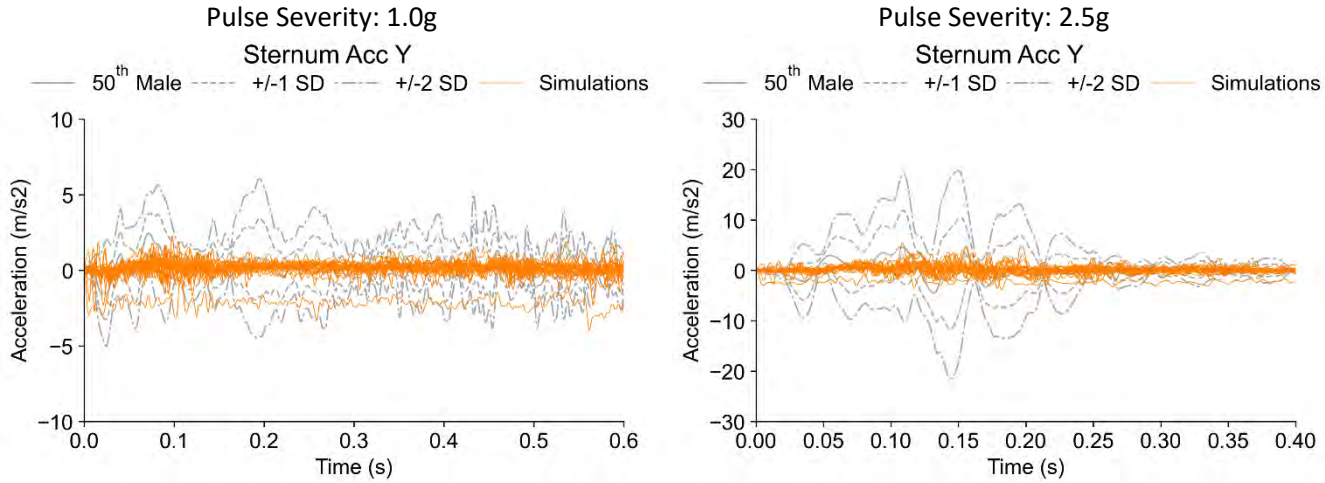

Fig. A 55. Comparison of Sternum Acc Y for all simulations with active muscles and experimental data (50th Male) for pre-crash braking (1g pulse severity: left) and low-speed impact event (2.5g pulse severity: right).

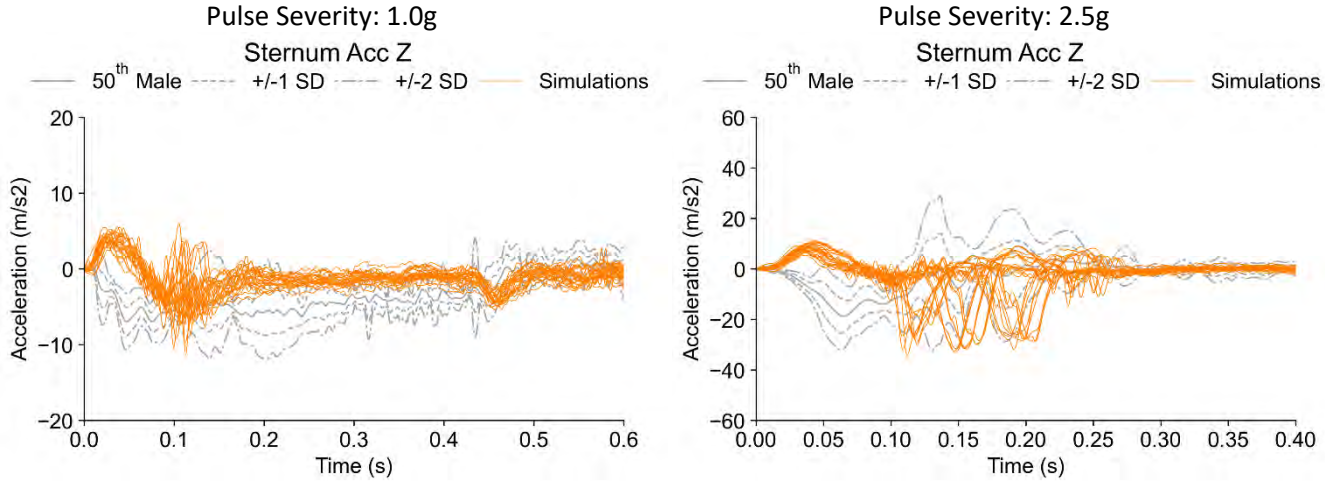

Fig. A 56. Comparison of Sternum Acc Z for all simulations with active muscles and experimental data (50th Male) for pre-crash braking (1g pulse severity: left) and low-speed impact event (2.5g pulse severity: right).

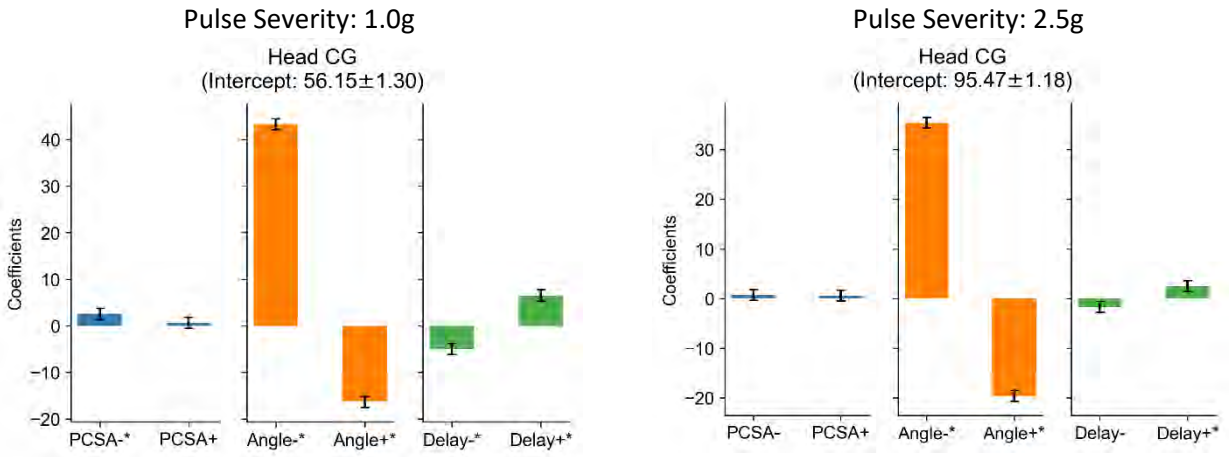

Fig. A57: Results of multivariate linear regression analysis for the head CG forward excursion for pre-crash braking (1g pulse severity: left) and low-speed impact event (2.5g pulse severity: right). Each subplot represents one independent variable category, each bar represents coefficients from the linear model, and the error bars show standard error. The coefficients are relative to the reference level in each category i.e. baseline value. X-ticks have * for statistically significant results.

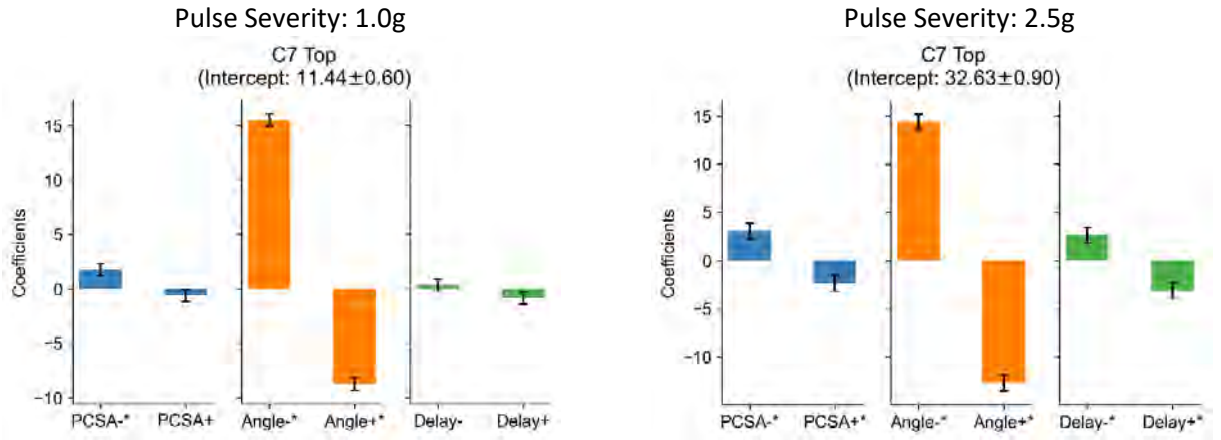

Fig. A58. Results of multivariate linear regression analysis for the C7 top forward excursion for pre-crash braking (1g pulse severity: left) and low-speed impact event (2.5g pulse severity: right). Each subplot represents one independent variable category, each bar represents coefficients from the linear model, and the error bars show standard error. The coefficients are relative to the reference level in each category i.e. baseline value. X-ticks have * for statistically significant results.

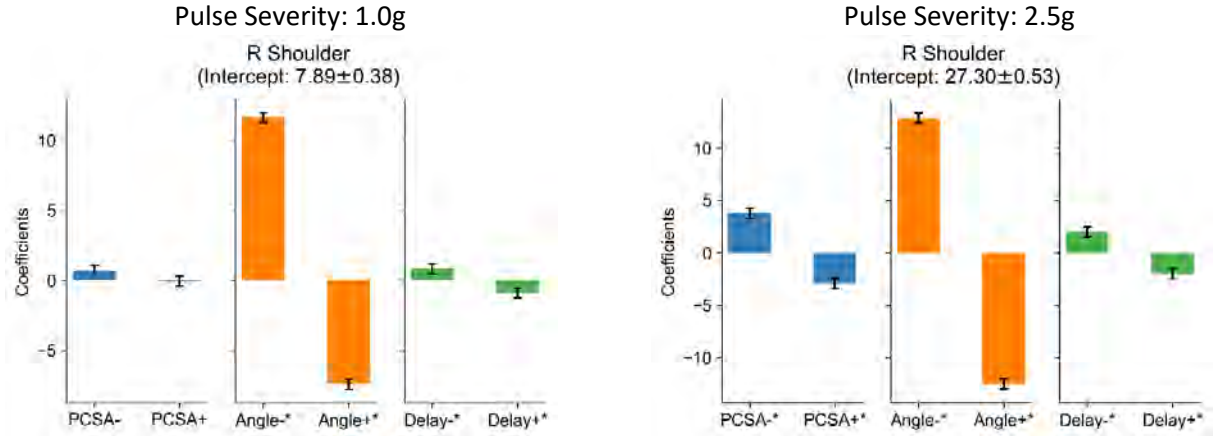

Fig. A59. Results of multivariate linear regression analysis for the right shoulder forward excursion for pre-crash braking (1g pulse severity: left) and low-speed impact event (2.5g pulse severity: right). Each subplot represents one independent variable category, each bar represents coefficients from the linear model, and the error bars show standard error. The coefficients are relative to the reference level in each category i.e. baseline value. X-ticks have * for statistically significant results.

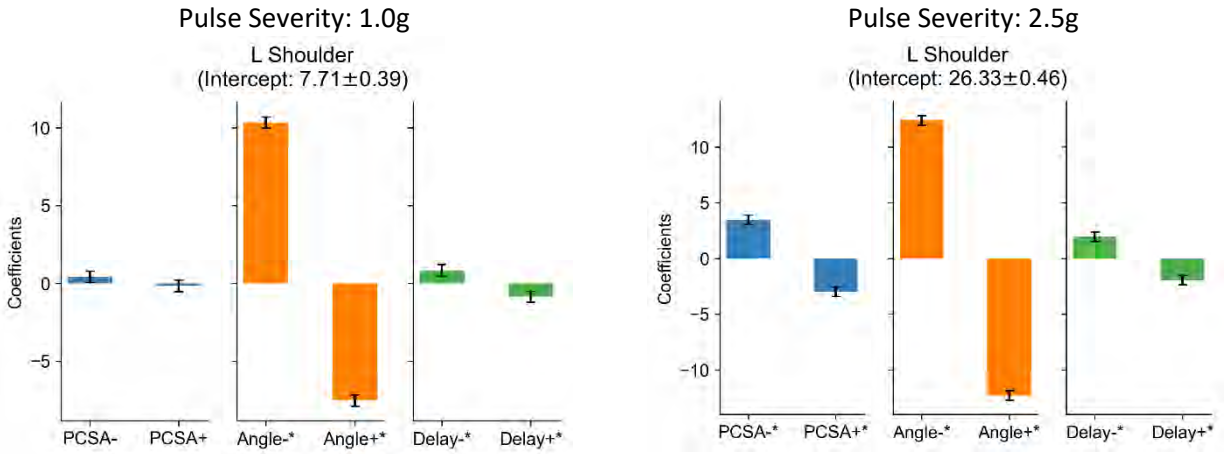

Fig. A60. Results of multivariate linear regression analysis for left shoulder forward excursion for pre-crash braking (1g pulse severity: left) and low-speed impact event (2.5g pulse severity: right). Each subplot represents one independent variable category, each bar represents coefficients from the linear model, and the error bars show standard error. The coefficients are relative to the reference level in each category i.e. baseline value. X-ticks have * for statistically significant results.

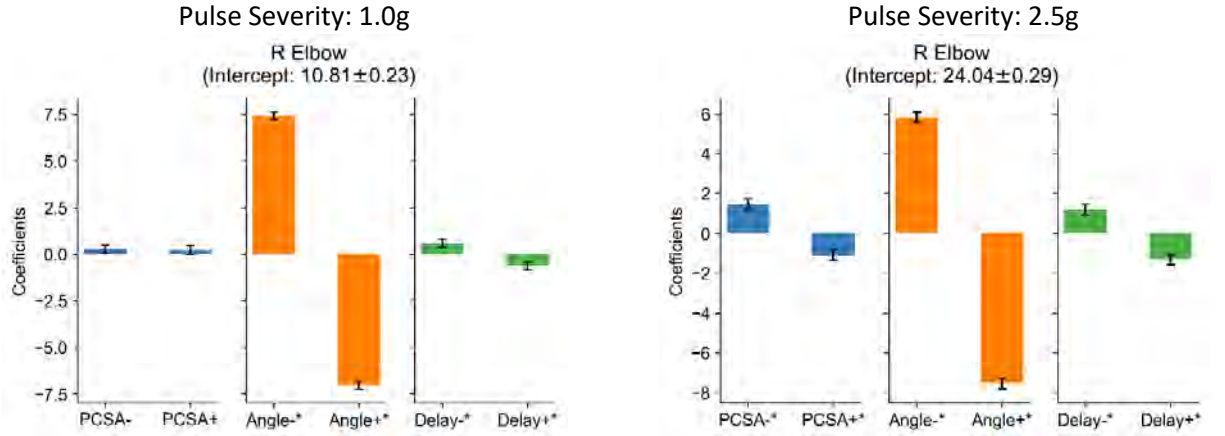

Fig. A61. Results of multivariate linear regression analysis for the right elbow forward excursion for pre-crash braking (1g pulse severity: left) and low-speed impact event (2.5g pulse severity: right). Each subplot represents one independent variable category, each bar represents coefficients from the linear model, and the error bars show standard error. The coefficients are relative to the reference level in each category i.e. baseline value. X-ticks have * for statistically significant results.

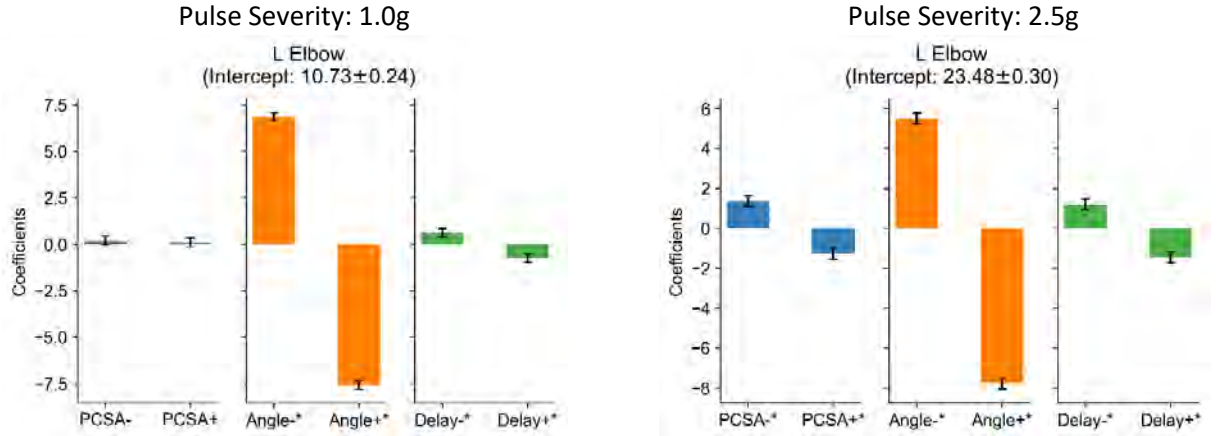

Fig. A62. Results of multivariate linear regression analysis for the left elbow forward excursion for pre-crash braking (1g pulse severity: left) and low-speed impact event (2.5g pulse severity: right). Each subplot represents one independent variable category, each bar represents coefficients from the linear model, and the error bars show standard error. The coefficients are relative to the reference level in each category i.e. baseline value. X-ticks have * for statistically significant results.

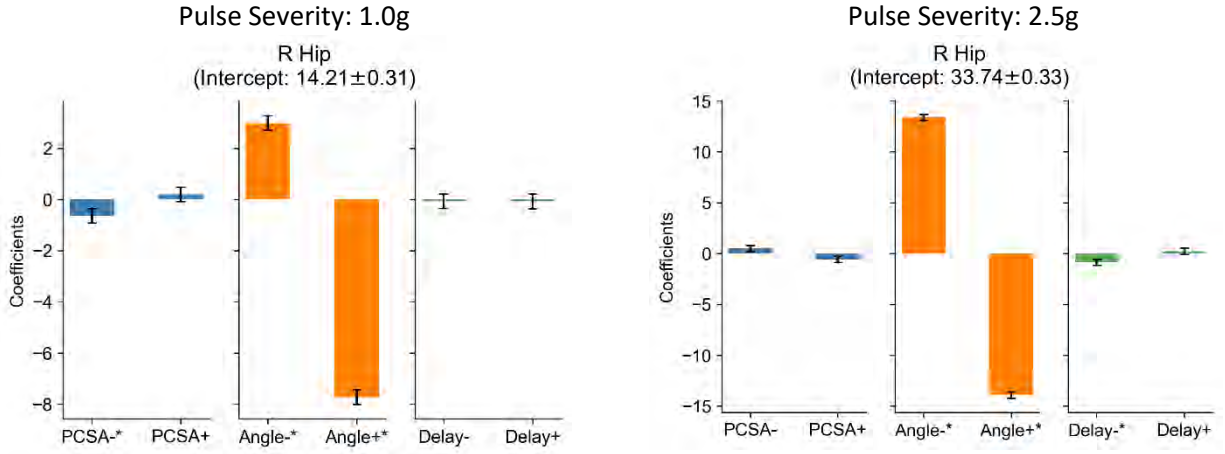

Fig. A63. Results of multivariate linear regression analysis for the right hip forward excursion for pre-crash braking (1g pulse severity: left) and low-speed impact event (2.5g pulse severity: right). Each subplot represents one independent variable category, each bar represents coefficients from the linear model, and the error bars show standard error. The coefficients are relative to the reference level in each category i.e. baseline value. X-ticks have * for statistically significant results.

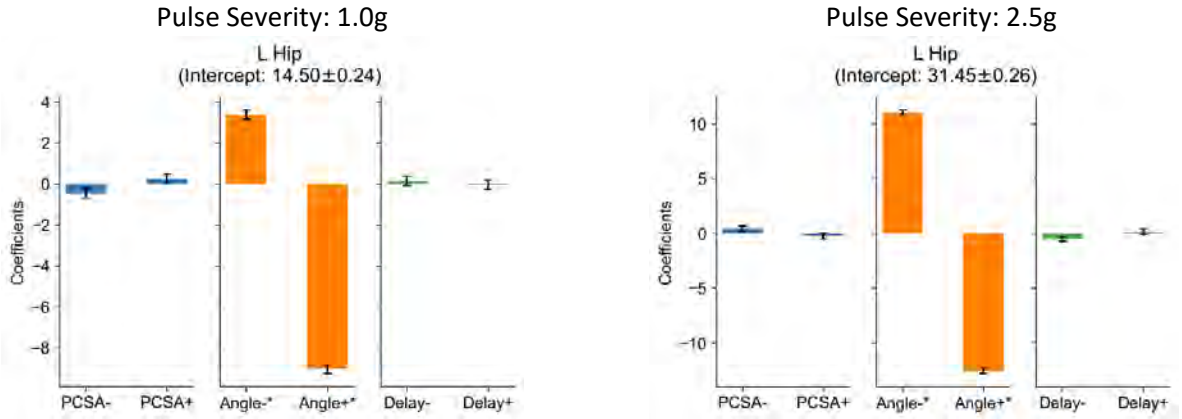

Fig. A64. Results of multivariate linear regression analysis for the left hip forward excursion for pre-crash braking (1g pulse severity: left) and low-speed impact event (2.5g pulse severity: right). Each subplot represents one independent variable category, each bar represents coefficients from the linear model, and the error bars show standard error. The coefficients are relative to the reference level in each category i.e. baseline value. X-ticks have * for statistically significant results.

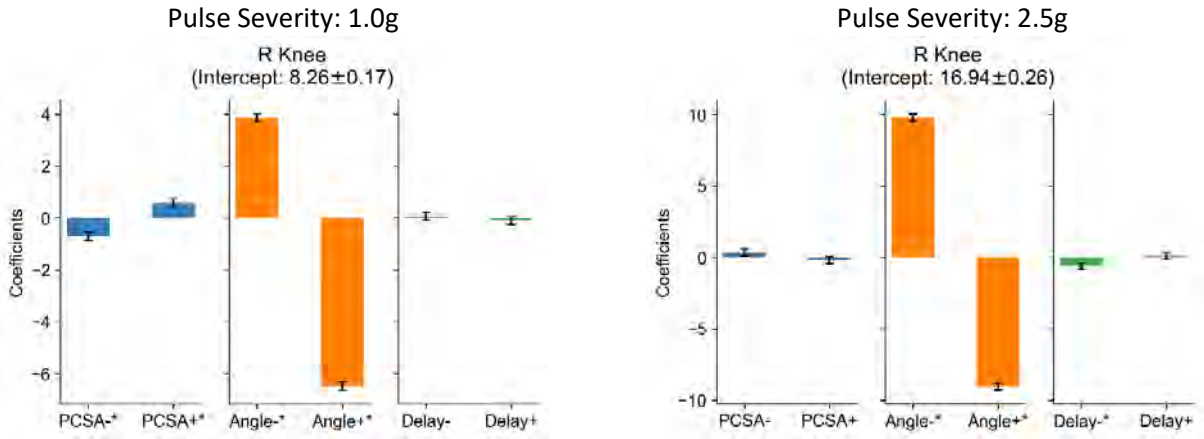

Fig. A65. Results of multivariate linear regression analysis for the right knee forward excursion for pre-crash braking (1g pulse severity: left) and low-speed impact event (2.5g pulse severity: right). Each subplot represents one independent variable category, each bar represents coefficients from the linear model, and the error bars show standard error. The coefficients are relative to the reference level in each category i.e. baseline value. X-ticks have * for statistically significant results.

Pulse Severity: 1.0g

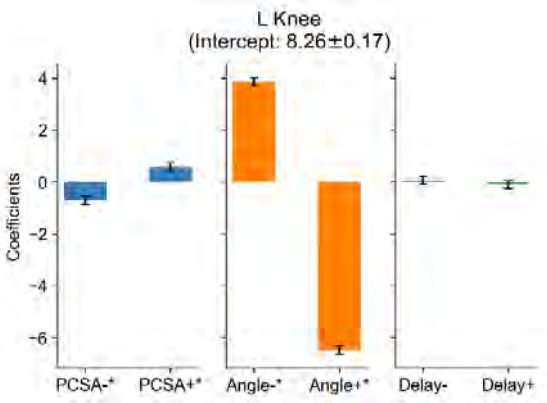

Pulse Severity: 2.5g

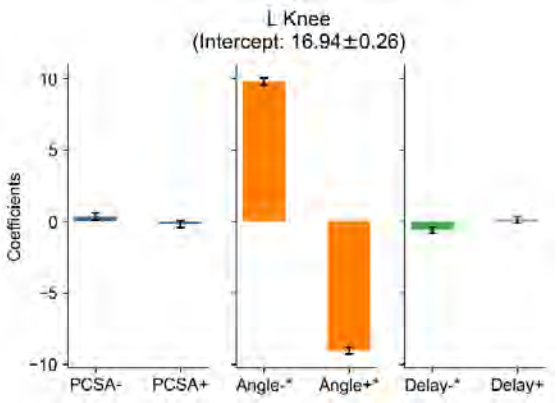

Fig. A66. Results of multivariate linear regression analysis for the left knee forward excursion for pre-crash braking (1g pulse severity: left) and low-speed impact event (2.5g pulse severity: right). Each subplot represents one independent variable category, each bar represents coefficients from the linear model, and the error bars show standard error. The coefficients are relative to the reference level in each category i.e. baseline value. X-ticks have * for statistically significant results.